

1 **Inferring Florida Current volume transport from satellite altimetry**

2 **Denis L. Volkov^{1,2}, Ricardo Domingues^{1,2}, Christopher S. Meinen², Rigoberto Garcia^{1,2},**
3 **Molly Baringer², Gustavo Goni², Ryan H. Smith²**

4 ¹Cooperative Institute for Marine and Atmospheric Studies, University of Miami, Miami,
5 Florida, USA.

6 ²NOAA Atlantic Oceanographic and Meteorological Laboratory, Miami, Florida, USA.

7 Corresponding author: Denis L. Volkov (denis.volkov@noaa.gov)

8 **Key Points:**

- 9 • Satellite altimetry can provide a useful but limited alternative for submarine cable
10 measurements of Florida Current volume transport
- 11 • Altimetry-derived transport adequately reproduces most transport changes, explaining
12 about 60% of the flow variance observed by the cable
- 13 • Altimetry is not endangered by severe weather, continuing to provide near-real time
14 transport estimates when in situ instruments may fail

Abstract

The nearly four-decades-long quasi-continuous daily measurements of the Florida Current (FC) volume transport at 27°N represents the longest climate record of a boundary current in existence. Given the extremely high utility of this submarine cable-collected time series for monitoring the Atlantic meridional overturning circulation, as well as for improving understanding and prediction of the regional weather, climate phenomena, coastal sea-level, and ecosystem dynamics, efforts are underway to establish a suitable backup observing system in case the cable becomes inoperable in the future. This study explores the utility of along-track satellite altimetry measurements since 1993 as a potential cable backup by establishing the relationship between the cross-stream sea surface height gradients and the FC volume transport derived from cable measurements and ship sections. We find that despite the lower temporal resolution, satellite altimetry can indeed serve as a decent but limited backup observing system. The FC transport inferred from satellite altimetry captures about 60% of the variability observed in the concurrent cable estimates, and the estimated error bars for the altimetry-derived transport are larger than those of the cable transport (2.1 Sv versus 1.5 Sv). We nevertheless demonstrate that satellite altimetry reproduces the seasonal, intra-seasonal, and inter-annual variability of the FC transport fairly well, as well as large transport anomalies during extreme weather events, such as tropical storms and hurricanes. The altimetry-derived transport can be provided in near-real time and serve the need to fill in data gaps in the cable record and assess its quality over time.

Plain Language Summary

Florida Current is one of the major conduits of heat, salt, carbon, nutrients and other properties in the subtropical North Atlantic, with profound influences on regional weather, climate, sea-level, and ecosystems. Daily monitoring of the Florida Current volume transport with a submarine cable has been maintained nearly continuously since 1982. Because of the extremely high value of these measurements for Earth system studies, efforts are underway to find a suitable backup observing system for the inevitable future when the cable fails. Satellites have been providing accurate measurements of sea level for nearly three decades. Due to the Earth's rotation, the direction of major oceanic currents is parallel to the lines of constant sea level, which for the Florida Current translates into sea level near the Bahamas being about 1-meter higher than sea level along Florida east coast. Variations in the Florida Current volume transport are linked to changes in the sea surface tilt across the Straits of Florida. This study demonstrates that accounting for the platform-specific limitations, satellite altimetry can serve as a limited but useful cable replacement, with the advantage of not being prone to damage from severe weather, which can often endanger the existing cable-based system.

1 Introduction

The Florida Current (FC) is the name given to the Gulf Stream as it passes through the Straits of Florida from the southernmost Florida Keys to the northernmost Bahamas Islands (Fig. 1). At 27°N, the FC has a mean transport of about 32 Sv (1 Sv = $10^6 \text{ m}^3 \text{ s}^{-1}$; e.g., Larsen and Sanford, 1985), and essentially fills the entire water column from the east coast of Florida to the west coast of Grand Bahama Island (Fig. 2a). The FC carries the majority of the upper-ocean northward transport of warm and saline waters in the subtropical North Atlantic at this latitude, and thus accounts for the bulk of both the upper limb of the Atlantic meridional overturning circulation and the western boundary component of the subtropical gyre circulation (e.g., Meinen

et al., 2010). Due to its proximity to land, importance for the maritime affairs, and impact on the coupled ocean-atmosphere system, observations of the FC date back to the late 1880s (e.g., Pillsbury, 1887; Stommel, 1957; Richardson and Schmitz, 1965; Niiler and Richardson, 1973; Molinari et al., 1985a).

A unique observing system for measuring the FC volume transport, T_{FC} , was established in 1982 as part of the Subtropical Atlantic Climate Studies project (e.g. Lee et al., 1985; Molinari et al., 1985b). It is based on a decommissioned submarine telecommunications cable between Florida and the Bahamas and ship sections along 27°N (Fig. 1a). As of today, the daily cable time series, T_{Cable} , provides the longest quasi-continuous climate record of a boundary current in existence, and it is a critical component of the trans-basin meridional overturning circulation observing array at 26.5°N (e.g. Johns et al., 2011; Frajka-Williams et al., 2019; Volkov et al., 2020). Abbreviations denoting the T_{FC} estimates used throughout the manuscript are listed in Table 1.

While the daily cable records are nearly continuous since 1982, some data gaps exist due to instrument failures as well as logistics or operational issues (Fig. 2b). The longest, 17-month gap occurred between October 1998 and March 2000, when the cable was retired from telephone service. Another long gap occurred in September-October 2004, when Hurricanes Frances and Jeanne damaged the building in which the recording system was housed. The most recent 1-month long gap occurred in July 2019 due to a voltage surge damaging the recording system in the Bahamas. Overall, from the beginning of cable observations in 1982 to May 2020, the gaps constituted about 10% of the entire record. Although the cable has been the most reliable and cost-effective measurement system for T_{FC} , there have been efforts to find a suitable backup and/or replacement system that would substitute the cable during inevitable future system failures and/or future cable breaks.

Geostrophic balance dictates that a strong boundary current co-evolves with a perpendicular (cross-stream) sea level gradient. The FC is associated with an average sea level difference between Florida and the Bahamas of about 0.7 m (Figs. 1b, 3). This suggests that sea level changes measured by tide gauges on either side of the Straits of Florida might be representative of changes in the transport (e.g., Schott and Zantopp, 1985). Because sea level gradients are directly related to the surface geostrophic velocity, relating these gradients to volume transports requires that the surface geostrophic velocity is a good predictor of velocity throughout the water column. This relationship was first studied by Maul et al. (1985), who reported on a high correlation ($r=0.95$) between the FC cable observations and monthly tide gauge records at Miami, Florida, and Cat Cay, Bahamas, although their study period was only 19 months (April 1982 through September 1983). Later, the same authors used a longer (1982-1988) daily time series and showed that sea level on the western side alone and sea level difference across the Straits of Florida can explain at least 60% of the FC transport variance in the subseasonal frequency band (Maul et al., 1990).

The use of tide gauges as a potential alternative to monitor T_{FC} is challenging, however, mainly because of the limited availability of continuous records across the FC, especially on the Bahamas side. Starting in 2008, the NOAA Atlantic Oceanographic and Meteorological Laboratory (AOML) has maintained and operated a pair of bottom pressure recorders (BPRs) deployed near the 12-m isobath on both sides of the Straits of Florida at 27°N as a potential alternative to monitor T_{FC} . Using the first six years of these observations (July 8, 2008 - September 17, 2014), Meinen et al. (2020) showed that the transports estimated from the pressure differences, T_{BPR} , explain roughly 55% of the total variance of T_{Cable} at time scales from

a few days to a year. They concluded that although the paired BPRs are ‘better than nothing’ for the cable backup/alternative observing system, they are not sufficient, and the potential utility of additional observations needs to be explored.

Along with tide gauges and BPRs, satellite altimetry is a component of the Global Ocean Observing System that provides periodic sea level measurements across the Straits of Florida along predetermined ground tracks (Fig. 1), and may provide a useful tool for monitoring the FC. The objective of this study is to explore the utility of along-track altimetry measurements to infer the FC volume transport. Unlike the submarine cable system, tide gauges, and shallow-water BPRs, satellite altimetry is not prone to weather conditions, and its quality is homogeneous throughout the almost 28 years of observations since 1993 (e.g., Pujol et al., 2016). Furthermore, satellite-altimetry boasts robust mission planning, with detailed launch schedules for instrument replacement, to ensure reliable and continuous measurements into the foreseeable future. It is, therefore, possible that satellite altimetry can be used (i) to fill in the existing gaps in the cable data record during the 1993 to present altimetry period; (ii) to evaluate the consistency of cable data quality over time; and (iii) to represent a feasible future replacement for the cable system. Therefore, the ultimate goal of this study is to derive the satellite-based transport estimates, $T_{\text{Altimetry}}$, and to evaluate its utility as a backup system for the cable measurements.

2 Data and Methods

2.1. Satellite altimetry

Satellite altimetry has provided accurate, continuous, and nearly global observations of sea level anomalies (SLA) since 1993 (e.g., Fu and Cazenave, 2001). The shortest repeat period for satellite overpasses is roughly 10 days, which means that the highly variable (on a day-to-day basis) FC is undersampled. While the sampling frequency of tide gauges and BPRs (usually hourly) is unsurpassable by remote sensing, altimetry satellites measure sea level variations at high spatial resolution along their ground tracks and, thus, yield the spatial structure of sea level gradients unavailable from small numbers of fixed-point sensors/moorings (Figs. 1b, 3). This makes it possible to objectively select only those satellite measurement locations that best compare with the cable-derived transport.

In this study, we use the along-track SLA from January 1993 to May 2020 with respect to a 20-year mean (1993-2012), processed and distributed by Copernicus Marine and Environment Monitoring Service (CMEMS; <https://marine.copernicus.eu/>). The along-track data is based on measurements by Topex/Poseidon (January 1993 - April 2002), Jason-1 (April 2002 - October 2008), Jason-2 (October 2008 - May 2016), and Jason-3 (May 2016 - present) satellites that have flown on the same orbit. We use both the delayed-time (January 1993 to October 2019) and near-real time (October 2019 - May 2020) data along two satellite tracks that cross the Florida Straits: the descending track 178 and the ascending track 243 (red dotted lines in Fig. 1). It takes approximately 80 seconds for a satellite to cross the Florida Straits from 25°N to 29°N. The along-track sampling interval is about 6.2 km.

The along-track SLA records include the Dynamic Atmospheric Correction (DAC), which accounts for (i) the high frequency oceanic response to meteorological forcing with periods less than 20 days, which is aliased by the altimetric measurements, and (ii) the low frequency inverse barometer response with periods greater than 20 days. The high frequency part is based on a barotropic model simulation forced by atmospheric pressure and winds (MOG2D; Lynch and Gray, 1979; Carrère and Lyard 2003). A 20-day cutoff-period was chosen because it corresponds

to the Nyquist period of T/P-Jason reference altimeters sampling and because the variability of sea level is mostly due to barotropic processes in this high frequency band. The application of DAC has been shown to improve the representation of sea level variability, in particular in coastal regions (e.g., Carrère and Lyard 2003; Volkov et al., 2007). On one hand, the high frequency part of the DAC accounts for significant wind-driven sea level fluctuations in the Straits of Florida, in particular near the coast, thus impacting the cross-strait sea level gradient directly linked to T_{FC} . Since the objective of this study is to link the daily estimates of T_{FC} with concurrent satellite measurements (snapshots), we add the DAC back to the along-track SLA. On the other hand, the low frequency inverse barometer response included in the DAC adds a signal not related to T_{FC} . However, because the spatial scale of sea level pressure changes is greater than the average width of the Straits of Florida (~100 km), this signal does not significantly affect the along-track sea level gradient across the FC. Overall, the application of DAC appears to have a rather small impact on the relationship between T_{Cable} and sea level gradient, with a correlation between these variables being only slightly (by 0.02) improved when the DAC is added back.

CMEMS provides the along-track SLA together with the Mean Dynamic Topography (MDT CNES-CLS18), computed for the time period 1993-2012 (Rio et al., 2018). The sum of SLA and MDT yields Sea Surface Height (SSH). The average along-track east-west SSH differences are about 70 cm for the track 178 and about 50 cm for the track 243 (Fig. 3). It should be noted that, between 25-26°N, track 243 lies approximately along the axis of the FC (Fig. 1b), which explains a relatively high along-track sea level to the west of 80°W compared to the track 178 (i.e., track 243 does not fully cross the FC between Florida and the Bahamas). The maximum variability of the along-track SSH is observed on either side of the FC, with standard deviations of about 10 cm (Fig. 3). This is consistent with the results of Meinen et al. (2020), who showed that the standard deviations of pressure recorded by the western and eastern BPRs at 27°N are close (0.34 and 0.32 dbar, respectively).

2.2. Florida Current measurements

The principles of electromagnetic induction, when applied to the ocean, dictate that when ions in seawater are advected by ocean currents through the Earth's magnetic field, an electric field is induced perpendicular to the direction of the water motion (Stommel, 1948; Sanford, 1971). Voltage perturbations induced on the cable by the varying FC flow are automatically recorded every minute, calibrated against other in situ observations, and processed into daily volume transport estimates, T_{Cable} (Larsen and Sanford, 1985; Larsen, 1992). Conversion of voltage into volume transport is done via linear transfer coefficients that were originally determined by comparison with direct ship-based volume transport estimates obtained at the cable site using Pegasus profilers (Spain et al., 1981). In the modern era, this ship section data is collected using free-falling dropsonde floats, $T_{Dropsonde}$ (red dots in Fig. 2b), and lowered acoustic Doppler current profilers (LADCP), T_{LADCP} (blue dots in Fig. 2b), at nine stations along 27°N line (e.g., Garcia and Meinen, 2014) (Fig. 1a). The methods involved in converting the cable voltages into daily transport estimates, as well as in calibrating and validating these estimates, have been well documented (e.g. Larsen and Sanford, 1985; Meinen et al., 2010; Garcia and Meinen, 2014). Starting from 2000, the cable measurements have been supported via the NOAA Western Boundary Time Series (WBTS) program, and the daily T_{Cable} estimates are available through the project's web page (www.aoml.noaa.gov/phod/wbts) (black curve in Fig. 2b). Although the transport time series are available with a daily temporal resolution, a three-day

lowpass filter is applied to the cable data as part of the standard processing for the removal of tides and high-frequency geomagnetic field variations. The reported accuracy of the daily cable measurements is 1.7 Sv and the decorrelation time scale is 10 days (Garcia and Meinen, 2014), which is close to the repeat period of Topex/Poseidon and Jason family of altimetry satellites.

In this paper, we focus on the cable data collected during the period also sampled by satellite altimetry, i.e. from January 1993 to May 2020 (Fig. 2b). During this time period, gaps in the cable time series resulting from various reasons constituted about 12% of the total length of the record. It should be noted that the quality of cable measurements is not homogeneous over time, with lower accuracy data having been collected during 1993-1998 when the submarine cable was in active use for telecommunications purposes (Larsen, 1991), and better but still problematic data collected during 2000-2005 due to issues with the recording system (Meinen et al., 2010). Comparison with the 227 dropsonde cruises conducted since 1993 illustrates this accuracy improvement. The root-mean-squared (RMS) differences between the dropsonde and cable estimates are 2.9 Sv in 1993-1998, 2.2 Sv in 2000-2005, and 1.5 Sv from 2006 to present. The LADCP measurements of the FC transport at 27°N started in 2001 (blue dots in Fig. 2b). Up to the present, there have been 80 LADCP cruises conducted with a frequency of 4-6 times a year. Although these measurements have not explicitly been used in the cable calibration, they are used to validate both the cable and dropsonde estimates. The RMS differences between the LADCP and cable estimates are 2.9 Sv in 2001-2005 and 1.6 Sv from 2006 to present.

2.3. Satellite altimetry sampling limitations

Topex/Poseidon and Jason family of altimetry satellites have provided SLA measurements along fixed groundtracks every 10 days in an uninterrupted fashion. This sampling, however, causes some limitations. First, while the along-track observations provide almost instantaneous snapshots of the FC cross-stream SSH gradient, some of the synoptic ocean variability with periods less than 20 days is inevitably missed by the altimeters. For example, a tropical storm or a hurricane can induce large fluctuations of sea level and volume transport in the Straits of Florida (e.g., Todd et al., 2018). While some of these events may be captured by a satellite overpass, they can also happen entirely between the satellite overpasses and be missed altogether. And second, since the FC transport and, hence, sea level across the Strait of Florida can change on a day-to-day basis, the undersampling by altimetry satellites may result in an aliasing of the high frequency variability into lower frequencies.

In order to obtain an initial assessment of potential misrepresentations with altimetry-derived estimates of T_{FC} as a result of the 10-day sampling interval, we subsampled T_{Cable} at the times of satellite overpasses during 1993-2020 (cyan curve in Fig. 2b). The subsampled T_{Cable} has a standard deviation of 3.2 Sv, only slightly lower than the 3.4 Sv of the standard deviation of the daily FC transport estimates (black curve in Fig. 3). If the 10-day subsampled time series is interpolated back to a daily time series, the RMS difference between the original and subsampled cable data is 2 Sv due to the omitted high-frequency variability and noise. The frequency spectra of the daily and 10-day transports (Fig. 4) start diverging at about 18 cycles per year (cpy), which is close to the Nyquist frequency of the 10-day estimates. At lower frequencies, the spectra are quite similar in terms of the signals and their power. There is a seasonal cycle consisting of the annual (~ 1 cpy) and semiannual (~ 2 cpy) harmonics. There are also notable peaks at ~ 2.8 and ~ 5.5 cpy (periods ~ 130 and ~ 66 days, respectively). At low frequencies (< 0.5 cpy), the 10-day subsampled T_{Cable} has somewhat more power than the daily T_{Cable} , but this difference is not statistically significant. The similar spectra, and the similar temporal standard

deviations, suggests that the potential aliasing of high frequency variability in the FC transport estimates using along-track satellite altimetry data with at 10-day sampling interval is probably small.

2.4. Florida Current and sea level

Geostrophy requires that any change in T_{FC} is related to a corresponding change of sea level tilt across the current. As noted in several previous studies (e.g. Ezer, 2015; Domingues et al., 2016), a stronger FC is associated with a lower sea level along Florida coast and a higher sea level on the Bahamas' side, and vice versa. This is illustrated by a diagram relating T_{Cable} to the along-track SSH (Fig. 5a). The diagram was constructed by sorting SSH profiles along the track 178 relative to the same day T_{Cable} in ascending order. In principle, such a diagram could be used as a lookup table to infer the FC volume transport for a given along-track SSH profile. In reality, however, this method does not produce robust results, mainly because one transport value is usually associated with more than one type/shape of the cross-stream SSH profile. When this is the case, the mean SSH profiles were used to plot the diagram. If no SSH profile exists for a particular transport value, which is mostly the case for extreme transport values (Fig. 5b), then linear interpolation between the nearest available profiles was used to fill in the gap. A Gaussian smoothing in both the longitude and the transport dimensions was also applied to reduce 'noise'. In addition, the number of SSH profiles for transports below ~ 27 Sv or above ~ 37 Sv is either small or zero (Fig. 5b), which increases uncertainties in the lookup table and complicates the robust reconstruction of extreme transport values. It is possible that continued observations and longer time series will eventually make this method more robust. As expected, the diagram illustrates the general tendency of the increasing SSH gradient with the increasing T_{Cable} . In addition, there is a tendency for higher sea levels along Florida east coast during the low T_{Cable} values.

An alternative way to proceed with inferring T_{FC} from satellite altimetry is to look for the maximum correlations between the cable transports and the along-track SSH. Prior to computing correlations, the along-track mean SSH between $25^{\circ}N$ and $30^{\circ}N$ was subtracted from each SSH value in order to remove the large-scale SSH variability not related to changes in the cross-stream SSH gradient. The 95% significance levels for correlations are based on the number of degrees of freedom, estimated by dividing the length of the time series by the integral time scale (Thomson and Emery, 2014). As expected, statistically significant (at 95% confidence) negative and positive correlations reaching ± 0.5 - 0.7 are observed to the west and to the east of the FC jet, respectively (Fig. 6). The absolute correlations obtained for track 178 are notably better than for track 243, meaning that the former better captures SSH variations linked with T_{Cable} . Similar to the comparison with dropsonde measurements mentioned above, correlations between T_{Cable} and the along-track SSH depend on the time interval considered. For the entire record (1993-2020), statistically significant (at 95% confidence) correlations are observed for both the track 178 ($r = \pm 0.5$ - 0.6) and the track 243 ($r = \pm 0.3$ - 0.5) (Fig. 6a). During 1993-1998, when there was the largest RMS difference (2.9 Sv) between the dropsonde and cable measurements, correlations between SSH and the cable transport were low and barely reached the 95% significance level, in particular for track 243 (Fig. 6b). In 2000-2005, correlations improved, reaching about ± 0.5 for both western and eastern segments of the track 178 and for the western segment of track 243 (Fig. 6c). The best correlations are observed in 2006-2018 reaching ± 0.6 - 0.7 for track 178 and ± 0.4 - 0.6 for track 243 (Fig. 6d). We note here that the differences in the obtained correlations

reflect changes in accuracy of T_{Cable} , since the quality of altimetry data remained stable throughout the entire delayed-time record.

Based on the better correlation with the cable transport, hereafter we focus on SSH records only along track 178. Furthermore, for exploring a statistical relationship between the along-track SSH and the cable transport, unless specified otherwise, we use the period 2006-2018, thus disregarding the periods when the cable transport was noisier (1993-2005) and the period when the available satellite altimetry data is of a near-real time quality (2019-2020). Similar to earlier studies (e.g. Meinen et al., 2020; Maul et al., 1985, 1990), we calculate sea level differences (ΔSSH) between the eastern and western parts of the Straits of Florida: $\Delta\text{SSH} = \text{SSH}_E - \text{SSH}_W$. However, we find that instead of using single measurement points to the east and to the west of the FC jet, e.g. the points of maximum correlations between the cable transport and SSH (Fig. 6), better results are obtained with SSH averaged over the eastern segment 79-79.5°W (SSH_E) and the western segment 80-80.5°W (SSH_W) along track 178 relative to the FC jet.

3 Results and Discussion

3.1. Altimetry-derived estimate of the Florida Current volume transport

The correlation between the normalized (by subtracting the mean and dividing by standard deviation) time series of T_{Cable} and ΔSSH in 2006-2018 (Fig. 7a) is 0.75, which is significant at 95% confidence level. This correlation coefficient is nearly the same as the one ($r=0.76$) obtained by Meinen et al. (2020), who used the differences between two pressure gauges deployed on either side of the Straits of Florida at 27°N in 2008-2014. Using the 2008-2014 time interval, almost the same as in Meinen et al. (2020), the correlation between T_{Cable} and ΔSSH from altimetry increases to 0.79. This means that a linear relationship between these quantities can explain about two thirds of the variance in the 10-day sampled T_{Cable} . The scatter plot suggests that, on average, a 1 Sv change in the FC transport is related to about a 4 cm change in ΔSSH (Fig. 7b). Similar to Meinen et al. (2020), we find that the correlation between the cable transport and ΔSSH is higher ($r \sim 0.85$) in autumn (September through November) and winter (December through February) and lower ($r \sim 0.75$) in spring (March through May) and summer (June through August) (not shown). The reason for the seasonality in the relationship between the cable transport and ΔSSH is unclear and requires further investigation.

It is important to note that SSH_E and SSH_W contribute almost equally to the correlation between T_{Cable} and ΔSSH (Fig. 6 a,d). In 2006-2018, the correlation between SSH_W and T_{Cable} is -0.67 (Fig. 7c), and the correlation between SSH_E and T_{Cable} is 0.7 (Fig. 7d). On average, a 1 cm change in either SSH_E or SSH_W is associated with a corresponding 0.4 Sv change in T_{Cable} . Both SSH_W and SSH_E are also significantly correlated with each other ($r = -0.68$), and on average a 3 cm change in SSH_W is associated with a 2 cm change in SSH_E with the opposite sign (Fig. 7e). In contrast, Maul et al. (1985) reported low correlations between the cable transport and sea level measured by a tide gauge at Cat Cay, Bahamas (25.55°N, 79.28°W) and by a BPR deployed at Memory Rock, Bahamas (26.95°N, 79.12°W). Meinen et al. (2020) also observed low correlation of 0.25 for the eastern BPR (27°N, 79.15°W) deployed at about 12-m depth in the Little Bahama Bank in 2008-2014. It is important to note that tide gauges and the two BPRs are representative for shallow waters only, while SSH_E is representative for the deep part of the Straits of Florida (Fig. 1a). Furthermore, the Cat Cay tide gauge is situated about 70 nautical miles south of the cable and, therefore, it does not account for the flow through the Northwest Providence Channel that also contributes to the variability in T_{FC} (e.g. Beal et al., 2008; Domingues et al., 2019).

Nevertheless, our result does not contradict Meinen et al. (2020), because the low correlation they observed for the eastern BPR, deployed at the Little Bahama Bank, is consistent with the low correlation ($r \cong 0.3$) estimates along track 243 at the location where it hits the Little Bahama Bank at around 79.3°W (Fig. 1a, 6d).

For the final linear regression to calibrate ΔSSH into the corresponding transport, we used the period 2008-2014, which is similar to the period studied in Meinen et al. (2020), and for which we estimated the relatively high correlation between T_{Cable} and ΔSSH ($r = 0.79$). The obtained linear regression coefficients were used to estimate $T_{Altimetry}$ from ΔSSH for the entire satellite altimetry record available to date (1993-2020) (cyan curve in Fig. 8). The resulting formula for the altimetry-based estimate is:

$$T_{Altimetry} = 26.13 \times \Delta SSH + 15.76 \quad (1),$$

where the units are meters for ΔSSH and Sverdrups (Sv) for $T_{Altimetry}$. The correlation coefficient between the 10-day subsampled T_{Cable} and $T_{Altimetry}$ for the entire record (1993-2020) is 0.63, which means that only about 40% of the variance is explained. This relatively small number is mostly due to a noisier cable signal in 1993-1998, during which the correlation between T_{Cable} and $T_{Altimetry}$ is 0.38. The correlation increases to 0.55 and 0.75 for the periods 2000-2005 and 2006-2020, respectively. These numbers are consistent with the inhomogeneous cable data quality discussed in section 2.2. It should be noted that T_{Cable} and $T_{Altimetry}$ are not fully independent for the period of linear regression (2008-2014), as the choice of the period affects both the slope and the offset of the linear regression. Nevertheless, the correlation for the fully independent estimates in 2015-2020 is similar ($r=0.76$). Furthermore, note that the last eight months of altimetry data (October 2019 - May 2020) are of the near-real time quality as opposed to the more accurate delayed-time data. It should be noted that the correlation between T_{Cable} and $T_{Altimetry}$ during these months ($r=0.73$) is only slightly lower than the correlations in prior periods of the same duration. This suggests that the altimetry transport estimates can be successfully obtained as soon as the near-real time altimetry data becomes available.

3.2. Validation and accuracy

Excluding the period when the cable was actively used for telecommunication (in the 1990s) and the period used for linear regression (2008-2014), the RMS difference between T_{Cable} and $T_{Altimetry}$ in 2001-2020 is 2.6 Sv. It is reasonable to assume that the transport estimates during this period are independent, so that the RMS difference between them represents the total error, ϵ_{total} , determined as the square root of the sum of the individual errors squared. Therefore, the accuracy of the altimetry-derived transport estimate, $\epsilon_{altimetry}$, becomes

$$\epsilon_{altimetry} = (\epsilon_{total}^2 - \epsilon_{cable}^2)^{1/2} \quad (2),$$

where ϵ_{cable} is the error of T_{Cable} . Although the accuracy of T_{Cable} has been reported as 1.7 Sv using the dropsonde sections and 1.8 Sv using the LADCP sections (Garcia and Meinen, 2014), these estimates can be updated with more recent data. If the dropsonde sections used for calibrating the cable voltages are excluded, then from 2001 to 2020, the RMS difference between the 93 independent dropsonde section transports (red circles in Fig. 2b and 8), and the concurrent daily cable-derived transports is 1.7 Sv ($r=0.78$). The RMS difference between the 80 independent LADCP section transports (blue circles in Fig. 2b and 8) and the concurrent cable-derived transports is 2 Sv ($r=0.81$). The estimated accuracies of the direct measurements of $T_{Dropsonde}$ and T_{LADCP} ($\epsilon_{dropsonde}$ and ϵ_{LADCP}) are 0.8 and 1.3 Sv, respectively (Garcia and Meinen,

2014) (Table 2). Subtracting these individual error bars of the section transports squared from the RMS differences squared and taking the square root yields the updated accuracy of T_{Cable} of 1.5 Sv: $\epsilon_{\text{cable}} = (1.7^2 - 0.8^2)^{1/2} = 1.5$ Sv using the dropsonde sections and $\epsilon_{\text{cable}} = (2.0^2 - 1.3^2)^{1/2} \sim 1.5$ Sv using the LADCP sections. Plugging the obtained cable error into equation (2), the accuracy of $T_{\text{Altimetry}}$ becomes: $\epsilon_{\text{altimetry}} = (2.6^2 - 1.5^2)^{1/2} \sim 2.1$ Sv (Table 2).

Similar to what is routinely done with the cable data, the altimetry-derived transport can be validated with independent quasi-instantaneous transports estimated from ship sections at 27°N (red and blue circles in Fig. 8). While a satellite flies across the FC in just about one minute (thus yielding instantaneous $T_{\text{Altimetry}}$), a dropsonde section takes approximately 6 hours and an LADCP section takes approximately 12 hours. In order to collocate $T_{\text{Altimetry}}$ with the direct measurements of $T_{\text{Dropsonde}}$ and T_{LADCP} , for each satellite overpass, we searched for ship sections that were conducted within ± 48 -hour window around the overpass hour. The choice of the window width is a trade-off between trying to find cruises as close as possible to the satellite overpass time and the total number of sections occupied within the specified window. For the 2001-2019 time interval, excluding the dropsonde sections that were used to calibrate cable voltages as well as the period of the near-real time altimetry data, a total of 32 dropsonde and 30 LADCP sections were identified for use in validating $T_{\text{Altimetry}}$. As illustrated in Fig. 9 and confirmed by quantifying statistics in Table 3, the scatter between the section transports and the 10-day subsampled T_{Cable} (blue squares in Fig. 9) is tighter than the scatter between the section transport measurements and $T_{\text{Altimetry}}$ (red circles in Fig. 9). Likewise, the correlations and RMS differences between the section and cable estimates are better than between the section and altimetry estimates.

Using the section transports, it is possible to obtain another estimate of the accuracy of $T_{\text{Altimetry}}$. Because the section and altimetry-derived transports are independent from each other, the RMS differences between them (the last column in Table 3) or the total error of transport estimates is determined as follows:

$$\epsilon_{\text{total}} = \begin{cases} (\epsilon_{\text{altimetry}}^2 + \epsilon_{\text{dropsonde}}^2 + \delta^2)^{1/2} \\ (\epsilon_{\text{altimetry}}^2 + \epsilon_{\text{LADCP}}^2 + \delta^2)^{1/2} \end{cases} \quad (3),$$

where δ is the random error due to the mismatch of satellite overpass times and the times of section occupations within the ± 48 -hour windows (collocation error). The collocation error is independent on the observing method (dropsonde or LADCP), and it is determined only by how much the FC transport can change within the specified window around the satellite overpass time. In order to estimate δ , for each daily cable transport value from 2006 to present, we computed the difference between this value and another randomly picked value within the ± 2 -day window around the former (i.e., randomly picking one out of 5 transport values per window). The RMS of the obtained differences yields the collocation error $\delta = 1.6$ Sv. Using equation (3), the accuracy of the altimetry-derived transport then becomes: $\epsilon_{\text{altimetry}} = (2.7^2 - 0.8^2 - 1.6^2)^{1/2} \sim 2.0$ Sv for the dropsonde sections and $\epsilon_{\text{altimetry}} = (2.8^2 - 1.3^2 - 1.6^2)^{1/2} \sim 1.9$ Sv for the LADCP sections. These estimates are consistent with the more conservative estimate obtained comparing the altimetry-derived transport to the cable transport (2.1 Sv) (Table 1). Overall, the accuracy of the altimetry-derived transport is close to the estimated accuracy of 2.7 Sv for the daily Florida Current transport determined using differences between the two BPRs deployed in the Straits of Florida (Meinen et al., 2020). We note that one of the possibilities to

refine the accuracy of $T_{\text{Altimetry}}$ in the future is to carry out dropsonde and LADCP sections during the days of satellite overpasses thus minimizing the collocation error.

3.3. Representation of the Florida Current variability

Having validated the altimetry-derived transport and evaluated its accuracy, it is instructive to investigate how well the obtained time series captures the variability of the daily FC transport inferred from the cable measurements at different time scales. Here, we focus on the following time scales: (i) the seasonal cycle, composed of the annual and semi-annual harmonics, (ii) the intra-seasonal variability with periods from 20 days to 1 year excluding the seasonal cycle, and (iii) the inter-annual variability with periods longer than 1.5 years. For comparison, the altimetry-derived transport was linearly interpolated to daily resolution to match the cable-derived transport. In order to avoid parts of the cable record with long data gaps, only the period 2005-2020 was considered, during which linear interpolation was used to fill in shorter data gaps. To account for possible nonstationarity of the signals, a magnitude-squared wavelet coherence between these transport estimates was computed using the analytic Morlet wavelet (Grinsted et al., 2004) and plotted in a time-period plane (Fig. 10). The phase of the wavelet cross-spectrum values was also computed to identify the relative lag between the input signals (arrows in Fig. 10). Because of the altimetry 10-day repeat cycle, the wavelet coherence has no meaningful values at periods shorter than 20 days (~ 0.7 months).

Overall, there is a reasonable in-phase relationship between T_{Cable} and $T_{\text{Altimetry}}$ at almost all resolved scales. Particularly high coherence values (>0.8) can be seen at periods ~ 4 -12 months, which include the seasonal cycle. There are relatively large patches of low coherence values (<0.5) in 2005-2006 and in 2013-2014 at periods shorter than 6 months, and in 2005-2011 at periods ~ 12 -24 months. Nevertheless, it is remarkable that many high-frequency signals with periods ranging from 20 days to 4 months as well as interannual signals present in the cable data are captured by satellite altimetry. For a more detailed comparison of the individual time scales of the variability, we reconstructed T_{FC} anomalies by inverting the continuous wavelet transforms of T_{Cable} and $T_{\text{Altimetry}}$ over the following ranges of periods: 170-195 days for the semi-annual and 345-385 days for the annual components of the seasonal cycle (Fig. 11a), 20-385 days for the intra-seasonal variability with the seasonal cycle (semi-annual + annual components) subtracted (Fig. 11b), and greater than 540 days for the inter-annual variability (Fig. 11c). The quantifying statistics for these scales of variability are presented in Table 4. One can see that all considered time scales of T_{Cable} variability are reasonably well reproduced by satellite altimetry measurements. The time series of T_{Cable} and $T_{\text{Altimetry}}$ associated with the seasonal, interannual, and intra-seasonal signals are significantly correlated at 95% confidence level (Fig. 11, Table 4).

The seasonal variability appears to be somewhat stronger in altimetry data with a standard deviation of 1.1 Sv compared to 0.9 Sv in the cable data (Fig. 11a). This is mostly due to the larger amplitude of the annual rather than semi-annual variability in $T_{\text{Altimetry}}$. The standard deviation of the annual variability in $T_{\text{Altimetry}}$ is 0.8 Sv compared to 0.5 Sv in T_{Cable} , while the standard deviations of the semi-annual variability of T_{Cable} (0.7 Sv) and $T_{\text{Altimetry}}$ (0.8 Sv) are similar (Table 4). It is not clear why the annual variability is more pronounced in the altimetry data. It appears that the spatial variations in the atmospheric pressure loading (inverted barometer effect included in the DAC) are not responsible for inducing the spurious annual variability in $T_{\text{Altimetry}}$, because we found no significant sensitivity of the annual variability to the application of the DAC in altimetry data. The intra-seasonal variability (Figure 11b) is the largest signal in T_{FC} and, as expected, the RMS difference between T_{Cable} and $T_{\text{Altimetry}}$ at this time scale is also

large (1.8 Sv) (Table 4). Nevertheless, $T_{\text{Altimetry}}$ adequately reproduces T_{Cable} at this time scale, and the two time series are significantly correlated ($r=0.67$).

The interannual variability of T_{Cable} in 2005-2020 was rather small with a standard deviation of 0.7 Sv (Table 4). It is reasonably well reproduced with $T_{\text{Altimetry}}$, but only starting from 2009 (Fig. 11c). The yearly averages of T_{FC} estimates in 1993-2020 (Fig. 12) reveal that most of the discrepancies between them in 2004-2020 are within the error bars besides an anomaly in 2007, when $T_{\text{Altimetry}}$ is significantly lower than T_{Cable} . The comparison between the yearly averages of T_{Cable} and $T_{\text{Altimetry}}$ in 1993-2003 is quite poor, although the differences are still within the error bars in 1993-1996. The observed differences in these years could be (i) due to the cable data quality, since the quality of altimetry data is homogeneous, and/or (ii) due to processes that were reflected in the altimeter SSH, but did not translate to the FC volume transport. It is interesting to note that during the large dip observed in 1999-2000 (Fig. 12), when the cable data had the longest gap, $T_{\text{Altimetry}}$ was well supported by the dropsonde section transports (rec circles in Fig. 8).

3.4. Representation of extreme events: Hurricanes Sandy (2012) and Dorian (2019)

One of the most important advantages of satellite altimetry over in-situ instrumentation is that it is not prone to damage from severe weather. Extreme weather events, such as tropical storms or hurricanes, can damage or destroy in-situ instruments, leading to data gaps or even to the complete termination of an observational program if the replacement of instruments is not possible or costly. Although near-surface moored instruments are the most vulnerable (e.g., tide gauges), the FC cable records have also been affected through damages inflicted on coastal infrastructure (i.e., the cable voltage recording system). Severe weather is often associated with very strong anomalies in the FC volume transport, which can pass unrecorded if the in-situ instrumentation is damaged. When weather is unfavorable, it is also not feasible to carry out any ship sections. Therefore, it is of particular interest and value to explore to what extent satellite altimetry could substitute for the cable and ship measurements during extreme weather events.

The record minimum FC volume transport of 17.1 Sv was measured by the cable on September 4, 2019, when Hurricane Dorian was hovering for a few days over the northern Bahamas Islands (Ezer, 2020; Volkov et al., 2020). Despite the very unfortunate and extensive devastation seen in the Bahamas, fortunately for observations there was neither damage to the building housing the cable voltage recording equipment nor a power outage that would stop the recording. Before the passage of Hurricane Dorian in 2019, the previous record minimum FC transport of 17.2 Sv was measured on October 28, 2012, when Hurricane Sandy was also travelling along the U.S. east coast northward without inflicting any damage to the recording equipment in the Bahamas. It should be noted, however, that given the accuracy of cable estimates (1.5 Sv), the difference between the minima T_{Cable} measured during these two hurricanes is statistically insignificant.

The daily time series of T_{Cable} and the 10-day time series of $T_{\text{Altimetry}}$ in 2012 (Fig. 13a) and in 2019 (Fig. 13b) illustrate a good agreement between the estimates during these two hurricane events. The full amplitude high-frequency variability in T_{Cable} forced by these hurricanes and captured is inevitably missed by satellites due to the 10-day sampling interval. However, it is clear that satellite altimetry was still able to capture the major tendencies and the large anomalies associated with Hurricanes Sandy and Dorian in particular. The passage of these hurricanes was characterized by abrupt reductions in T_{Cable} and then more gradual recoveries complicated by aftereffects represented by sequences of negative anomalies. Although there was no satellite

overpass close to the minimum T_{Cable} caused by Hurricane Sandy on October 28, 2012, satellite altimetry successfully observed low transports on November 11 and November 21, 2012 (blue and red dots in Fig. 13a; see also Table 5). By that time Hurricane Sandy had already dissipated, and the observed anomalies in T_{Cable} and $T_{\text{Altimetry}}$ were likely generated by coastally trapped waves traveling from the north, which are commonly triggered by weather events (e.g., Mooers et al., 2005; Todd et al., 2018; Ezer, 2020) or by ocean dynamics (e.g. Domingues et al, 2019). During Hurricane Dorian, there was a satellite overpass on September 5, 2019, i.e. a day after a record minimum T_{Cable} was reached. On this date the hurricane's eye was already positioned north of the Straits of Florida and to the east of Georgia and South Carolina. Nevertheless, the FC transport was still low, with T_{Cable} and $T_{\text{Altimetry}}$ estimates of 18.9 and 21.7 Sv, respectively (black dot in Fig. 13b; Table 5). Before the FC transport recovered after Hurricane Dorian, satellite altimetry successfully captured two negative transport anomalies in October and November (red and green dots in Fig. 13b). It should be noted that before Hurricane Dorian, there was a month-long gap in T_{Cable} due to a power surge in the Bahamas in July 2019 that destroyed the recording system. Satellite altimetry appears to adequately reconstruct the missing data. An LADCP section on July 10, 2019 yielded a transport of 34.7 Sv (blue cross in Fig. 13b in July), which compares reasonably to the 31.4 and 34.0 Sv estimated with altimetry on July 7 and July 17, respectively (cyan curve in Fig. 13b).

It is instructive to examine how the sea level slope along the satellite track 178 was changing over the dates around the passages of Hurricanes Sandy and Dorian (Fig. 13 c,d). In both cases, the strong decrease of the FC transport was associated with flattening of the along-track SSH gradient. The low transports observed by satellite altimetry on November 11 and 22, 2012 were associated with about 20-cm higher SSH to the west of the FC jet and about 20-cm lower SSH to the east of the FC jet compared to SSH observed on October 2, 2012, before the arrival of Hurricane Sandy. Similarly, Hurricane Dorian led to a partial destruction of the SSH gradient across the Straits of Florida, which is well reflected in the along-track SSH gradient (Fig. 13d) associated with the lowest $T_{\text{Altimetry}}$ (21.7 Sv; Table 5) observed on September 5, 2019. This caused higher-than-usual sea-levels along the southeast coast of Florida and led to extensive flooding directly and/or indirectly forced by the hurricane.

Interestingly, the SSH gradient on September 5, 2019 even implies a southward geostrophic flow at about 80°W (black curve in Fig. 13d). Luckily, weather conditions in the Strait of Florida on September 6, 2019 permitted us to carry out a dropsonde section, during which expendable BathyThermograph (XBT) probes were also launched. The depth-integrated velocities estimated from dropsonde measurements also reveal a southward flow of about 35 cm/s at the westernmost station (Fig. 14a). Consistent with the dropsonde measurements, the meridional geostrophic velocities relative to the bottom calculated from the XBT temperature profiles and empirically-derived salinity profiles (Fig. 14b) confirm the presence of the southward near-surface flow from the coast of Florida to about 79.75°W and show an eastward shift of the FC jet towards approximately 79.45°W (compare to the mean state shown in Fig. 2a). This example illustrates a remarkable consistency between the three totally independent observing methods. Overall, it is possible to summarize that although the fast nature of the movements of tropical storms and hurricanes demonstrates a limitation of the 10-day sampling of satellite altimetry, the altimetry-derived SSH gradients do still appear to be useful for examining the ocean state in the Straits of Florida during extreme weather events.

4 Conclusions

The results presented herein indicate that satellite altimetry is a useful tool for monitoring the FC. While the temporal resolution of satellite altimetry records is limited, and only allows the resolution of signals with periods greater than 20 days, satellite altimetry has the advantage of providing details of the spatial structure of the sea level gradient across the FC. Altimetry-based estimates of the FC volume transport have been obtained from the linear regression of the cable transport estimates on the cross-flow SSH differences along the descending track 178 of Topex/Poseidon and Jason series satellites. We find that these estimates can capture roughly 60% of the total variance observed by the cable.

Separating the results out into differing time scales, we have demonstrated that the altimetry-derived transport reasonably reproduces the seasonal, intra-seasonal, and inter-annual variability. The annual and semi-annual components of the seasonal variability in the altimetry-derived transport in most cases match well those of the cable transport in terms of amplitude and phase. On average, however, the annual amplitude of the altimetry-derived transport is somewhat greater than that of the cable transport for the reasons that are not yet clear (subtracting the dynamic atmospheric correction from the altimetry data has been excluded as a potential reason for this amplitude disparity). The intra-seasonal variability is the strongest in both the cable- and altimetry-derived transport estimates. While the cable and altimetry-based estimates are significantly correlated ($r=0.67$) at these time scales, the latter underestimates the former by about 30%. The RMS difference between the two estimates (1.8 Sv) at intra-seasonal time scales is the largest among the time scales considered. The inter-annual variability of the cable transport is well reproduced by altimetry, but only starting from 2009. Earlier records exhibit substantial discrepancies that may result from poorer cable data quality, particularly before 2006. Despite being not able to resolve high-frequency signals with periods less than 20 days, satellite altimetry provides snapshot observations of SSH across the FC that may at times capture the very large transport fluctuations driven by the passage of tropical storms and hurricanes. We have shown that the two lowest FC cable transports on record occurred during Hurricanes Sandy and Dorian in 2012 and 2019, respectively, and these anomalous low transports were also reflected in satellite altimetry measurements.

With that, our results suggest that altimetry, like BPRs being maintained on both sides of the Straits of Florida at 27°N (Meinen et al., 2020), can provide a valuable resource for measuring the FC volume transport in the inevitable future when the cable fails, as well as being useful for filling in the already existing data gaps in the cable time series. The accuracy of the altimetry-based transport estimates is 2.1 Sv, which is based on the comparisons with the cable as well as with dropsonde and LADCP section-based estimates. As expected, this is slightly worse than the accuracy of the daily cable transport of 1.5 Sv. One way to better quantify the estimates of the accuracy of the altimetry-based FC transport estimates is to carry out ship sections specifically during the days of satellite overpasses, which we plan to do in the future. Nevertheless, with existing data, it is clear that the altimetry-based estimates can be used to fill gaps in the existing cable record, and they do represent a potential replacement system for the existing cable-based system should the latter fail.

Another advantage of satellite altimetry is that, unlike the cable recording system or near-surface in situ instrumentation (e.g., tide gauges and BPRs), satellite altimetry is not at risk from adverse weather conditions (e.g., tropical storms and hurricanes). Altimetry has provided gap-free and homogeneous-quality records since 1993. The consistent quality of the altimeter data has also allowed us to demonstrate that there are periods when the existing cable data themselves are more and less accurate. We have shown that the best comparison between the cable transport

and the cross-flow SSH differences is observed starting from 2006, while the 1993-2005 part of the cable record is noisier. This is consistent with the comparison between the cable- and independent ship section-based transport estimates, which also suggests a poorer cable data quality in 1993-2005.

Finally, although the overall performance of the altimetry-derived FC transport estimates provides a good representation of the variability in various timescales, it is not able to fully account for the variance observed in the cable data. This unexplained variance (~40%), which is mostly due to misrepresented intra-seasonal and inter-annual signals, might be resulting from the fact that the baroclinic and barotropic components of the flow through the Straits of Florida tend to vary independently (Meinen and Luther, 2016), and satellite altimetry measurements cannot distinguish between variations of one or the other component of the flow. Altimetry alone, therefore, is not sufficient for monitoring the FC volume transport with an accuracy similar to the cable. While dropsonde, LADCP, and hydrography sections remain vital for calibration/validation purposes and for observing the vertical structure of the FC, additional research is needed to evaluate what other observing system components might increase the variance captured when used together with altimetry.

Acknowledgments

The cable observations and ship section data (dropsonde/XBT and CTD/LADCP) have been supported by the U.S. NOAA Climate Program Office-Global Ocean Monitoring and Observing program via the Western Boundary Time Series (WBTS) project (FundRef number 100007298) and by the NOAA Atlantic Oceanographic and Meteorological Laboratory (AOML). The authors were supported by the WBTS project and by the AOML. DLV and RD were partially supported by NOAA's Climate Variability and Predictability program (grant number NA20OAR4310407). DLV, RD, and RG were also supported in part under the auspices of the Cooperative Institute for Marine and Atmospheric Studies (CIMAS), a cooperative institute of the University of Miami and NOAA, cooperative agreement NA10OAR4320143. Satellite altimetry data used in this study are distributed through the Copernicus Marine and Environment Monitoring Service (<https://marine.copernicus.eu/>). The Florida Current volume transports obtained from the cable measurements and ship sections are available from the WBTS project's web page (www.aoml.noaa.gov/phod/wbts). MDT CNES-CLS18 was produced by CLS and distributed by Aviso+, with support from CNES (<https://www.aviso.altimetry.fr/>).

References

- Beal, L. M., J.M. Hummon, E. Williams, O.B. Brown, W. Baringer, & E.J. Kearns (2008). Five years of Florida Current structure and transport from the Royal Caribbean Cruise Ship Explorer of the Seas. *J. Geophys. Res. Oceans*, 113(C6).
- Carrère, L., and F. Lyard (2003). Modelling the barotropic response of the global ocean to atmospheric wind and pressure forcing - Comparisons with observations, *Gephys. Res. Lett.*, 30, 1275–1278.
- Domingues, R., M. Baringer, & G. Goni (2016). Remote sources for year-to-year changes in the seasonality of the Florida Current transport. *J. Geophys. Res. Oceans*, 121(10), 7547-7559.
- Domingues, R. M., W.E. Johns, & C.S. Meinen (2019). Mechanisms of Eddy-Driven Variability of the Florida Current. *J. Phys. Oceanogr.*, 49(5), 1319-1338.
- Ezer, T. (2020). The long-term and far-reaching impact of hurricane Dorian (2019) on the Gulf Stream and the coast. *Journal of Marine Systems*, 208, 103370, doi:10.1016/j.jmarsys.2020.103370.
- Ezer, T. (2015). Detecting changes in the transport of the Gulf Stream and the Atlantic overturning circulation from coastal sea level data: The extreme decline in 2009–2010 and estimated variations for 1935–2012. *Global and Planetary Change*, 129, 23-36.
- Frajka-Williams E., I.J. Ansorge, J. Baehr, H.L. Bryden, M.B. Chidichimo, S.A. Cunningham, G. Danabasoglu, S. Dong, K.A. Donohue, S. Elipot, P. Heimbach, N.P. Holliday, R. Hummels, L.C. Jackson, J. Karstensen, M. Lankhorst, I.A. Le Bras, M.S. Lozier, E.L. McDonagh, C.S. Meinen, H. Mercier, B.I. Moat, R.C. Perez, C.G. Piecuch, M. Rhein, M.A. Srokosz, K.E. Trenberth, S. Bacon, G. Forget, G. Goni, D. Kieke, J. Koelling, T. Lamont, G.D. McCarthy, C. Mertens, U. Send, D.A. Smeed, S. Speich, M. van den Berg, D. Volkov and C. Wilson (2019). Atlantic Meridional Overturning Circulation: Observed Transport and Variability. *Front. Mar. Sci.* 6:260. doi: 10.3389/fmars.2019.00260.
- Fu, L.-L., and A. Cazenave (2001), *Satellite Altimetry and Earth Sciences: A Handbook of Techniques and Applications*, Int. Geophys. Ser., vol. 69, Academic, San Diego, Calif.
- Garcia, R.F., C.S. Meinen (2014). Accuracy of Florida Current volume transport measurements at 27°N using multiple observational techniques. *J. Atmos. Ocean. Tech.* 31(5):1169–1180. doi:10.1175/JTECH-D-13-00148.1.
- Grinsted, A. J., C. Moore, and S. Jevrejeva (2004). Application of the cross wavelet transform and wavelet coherence to geophysical time series. *Nonlinear Processes in Geophysics*. Vol. 11, Issue 5/6, 2004, pp. 561–566.
- Johns, W. E., M.O. Baringer, L.M. Beal, S.A. Cunningham, T. Kanzow, H.L. Bryden, J. J. M. Hirschi, J. Marotzke, C. S. Meinen, B. Shaw, R. Curry (2011). Continuous, array-based estimates of Atlantic Ocean heat transport at 26.5 N. *Journal of Climate*, 24(10), 2429-2449, doi: 10.1175/2010JCLI3997.1.
- Larsen, J.C., and T.B. Sanford (1985). Florida Current volume transports from voltage measurements. *Science*. 227:302–304.
- Larsen, J.C. (1992). Transport and heat flux of the Florida Current at 27°N derived from cross-stream voltages and profiling data: theory and observations. *Phil. Trans. R. Soc. Lond. A*. 338:169–236.

- 666 Lee, T.N., F.A. Schott, R. Zantopp (1985). Florida Current: low-frequency variability as
667 observed with moored current meters during April 1982 to June 1983. *Science* 227, 298–302.
- 668 Lynch, D. R., and W. G. Gray (1979), A wave equation model for finite element tidal
669 computations, *Comput. Fluids*, 7, 207–228, doi:10.1016/0045-7930(79)90037-9.
- 670 Maul, G.A., F. Chew, M. Bushnell, D.A. Mayer (1985). Sea level variation as an indicator of
671 Florida Current volume transport: comparisons with direct measurements. *Science*. 227:304–307.
- 672 Maul, G.A., D.A. Mayer, M. Bushnell (1990). Statistical relationships between local sea level
673 and weather with Florida-Bahamas cable and Pegasus measurements of Florida Current volume
674 transport. *J. Geophys. Res.* 95(C3):3287–3296.
- 675 Meinen, C.S., R.F. Garcia, R. Smith (2020). Evaluating pressure gauges as a potential future
676 replacement for electromagnetic cable observations of the Florida Current transport at 27°N. *J.*
677 *Oper. Oceanogr.*, doi:10.1080/1755876X.2020.1780757.
- 678 Meinen, C. S., and D.S. Luther (2016). Structure, transport, and vertical coherence of the Gulf
679 Stream from the Straits of Florida to the Southeast Newfoundland Ridge. *Deep-Sea Res. I*, 112,
680 137–157, doi:10.1016/j.dsr.2016.02.002.
- 681 Meinen, C.S., M.O. Baringer, R.F. Garcia (2010). Florida Current transport variability: an
682 analysis of annual and longer period signals. *Deep Sea Res. I*. 57:835–846.
683 doi:10.1016/j.dsr.2010.04.001.
- 684 Molinari, R.L., W.D. Wilson, K. Leaman (1985a). Volume and heat transports of the Florida
685 Current: April 1982 through August 1983. *Science* 227, 295–297.
- 686 Molinari, R.L., G.A. Maul, F. Chew, W.D. Wilson, M. Bushnell, D. Mayer, K. Leaman, F.
687 Schott, T. Lee, R. Zantopp, J.C. Larsen, T.B. Sanford (1985b). Subtropical Atlantic Climate
688 Studies: Introduction. *Science*, 227, 292–295.
- 689 Mooers, C. N. K., C. S. Meinen, M. O. Baringer, I. Bang, R. Rhodes, C. N. Barron, and F. Bub
690 (2005). Cross Validating Ocean Prediction and Monitoring Systems, *EOS*, 86(29), 269, 272–273,
691 doi:10.1029/2005EO290002.
- 692 Niiler, P.P. W.S. Richardson (1973). Seasonal variability of the Florida Current. *J. Mar. Res.* 31,
693 144–167.
- 694 Pillsbury, J.E. (1887). Gulf Stream Explorations – Observations of Currents – 1887. Rept. Supt.,
695 US Coast Geod. Surv., Appendix 8, 173–184.
- 696 Pujol, M.-I., Y. Faugère, G. Taburet, S. Dupuy, C. Pelloquin, M. Ablain, and N. Picot (2016).
697 DUACS DT2014: The new multi-mission altimeter data set reprocessed over 20 years. *Ocean*
698 *Science*, 12(5), 1067–1090. doi:10.5194/os-12-1067-2016.
- 699 Richardson, W.S., and W.J. Schmitz Jr. (1965). A technique for the direct measurement of
700 transport with application to the Straits of Florida. *J. Mar. Res.* 23, 172–185.
- 701 Schott, F., and R. Zantopp (1985). Florida Current: seasonal and interannual variability. *Science*.
702 227(4684):308–311.
- 703 Spain, P. F., D.L. Dorson, H.T. Rossby (1981). PEGASUS: a simple, acoustically tracked
704 velocity profiler. *Deep Sea Res.* 28A, 1553–1567.
- 705 Stommel, H. (1957). Florida Straits transports: 1952–1956. *Bull. Mar. Sci. Gulf Carib.* 7:252–
706 254.

- 707 Stommel, H. (1948). The theory of the electric field induced in deep ocean currents. *J. Mar. Res.*
708 7:386–392.
- 709 Todd, R. E., Asher, T. G., Heiderich, J., Bane, J. M., & Luetlich, R. A. (2018). Transient
710 response of the Gulf Stream to multiple hurricanes in 2017. *Geophys. Res. Lett.*, 45, 10,509–
711 10,519, doi:10.1029/2018GL079180.
- 712 Thomson, R.E., & W.J. Emery (2014). *Data analysis methods in physical oceanography*, 3rd
713 edition, Elsevier B.V., pp. 716.
- 714 Volkov, D.L., C.S. Meinen, C. Schmid, B. Moat, M. Lankhorst, S. Dong, F. Li, W. Johns, S.
715 Lozier, R. Perez, G. Goni, M. Kersale, E. Frajka-Williams, M. Baringer, D. Smeed, D. Rayner,
716 A. Sanchez-Franks, and U. Send (2020). Atlantic meridional overturning circulation and
717 associated heat transport [in “State of the Climate in 2019”]. *Bull. Amer. Meteor. Soc.*, 101 (8),
718 S163–S169, [https:// doi.org/10.1175/BAMS-D-20-0105.1](https://doi.org/10.1175/BAMS-D-20-0105.1).
- 719 Volkov, D. L., G. Larnicol, and J. Dorandeu (2007). Improving the quality of satellite altimetry
720 data over continental shelves, *J. Geophys. Res.*, 112, C06020, doi:10.1029/2006JC003765.

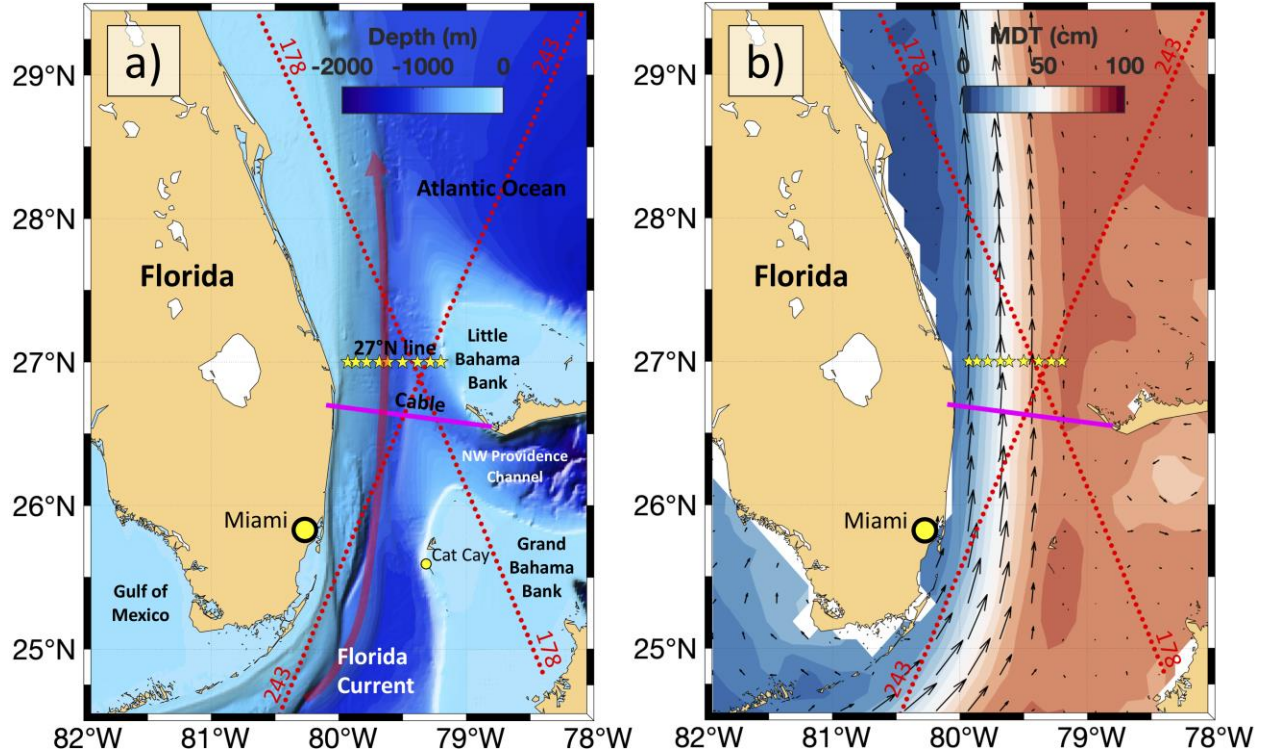


Figure 1. The Florida Current and its observing system components. (a) Bathymetric chart of the northern Straits of Florida: (magenta line) the submarine telephone cable between Florida and the Bahamas, (red dots) the descending track 178 and the ascending track 243 of Topex/Poseidon and Jason series satellites, (yellow stars) dropsonde and LADCP stations at 27°N. (b) The Mean Dynamic Topography, MDT CNES-CLS18 (color), and associated mean surface geostrophic velocity (arrows). The MDT CNES-CLS18 is an estimate of the mean SSH above the geoid over the 1993-2012 period (Rio et al., 2018).

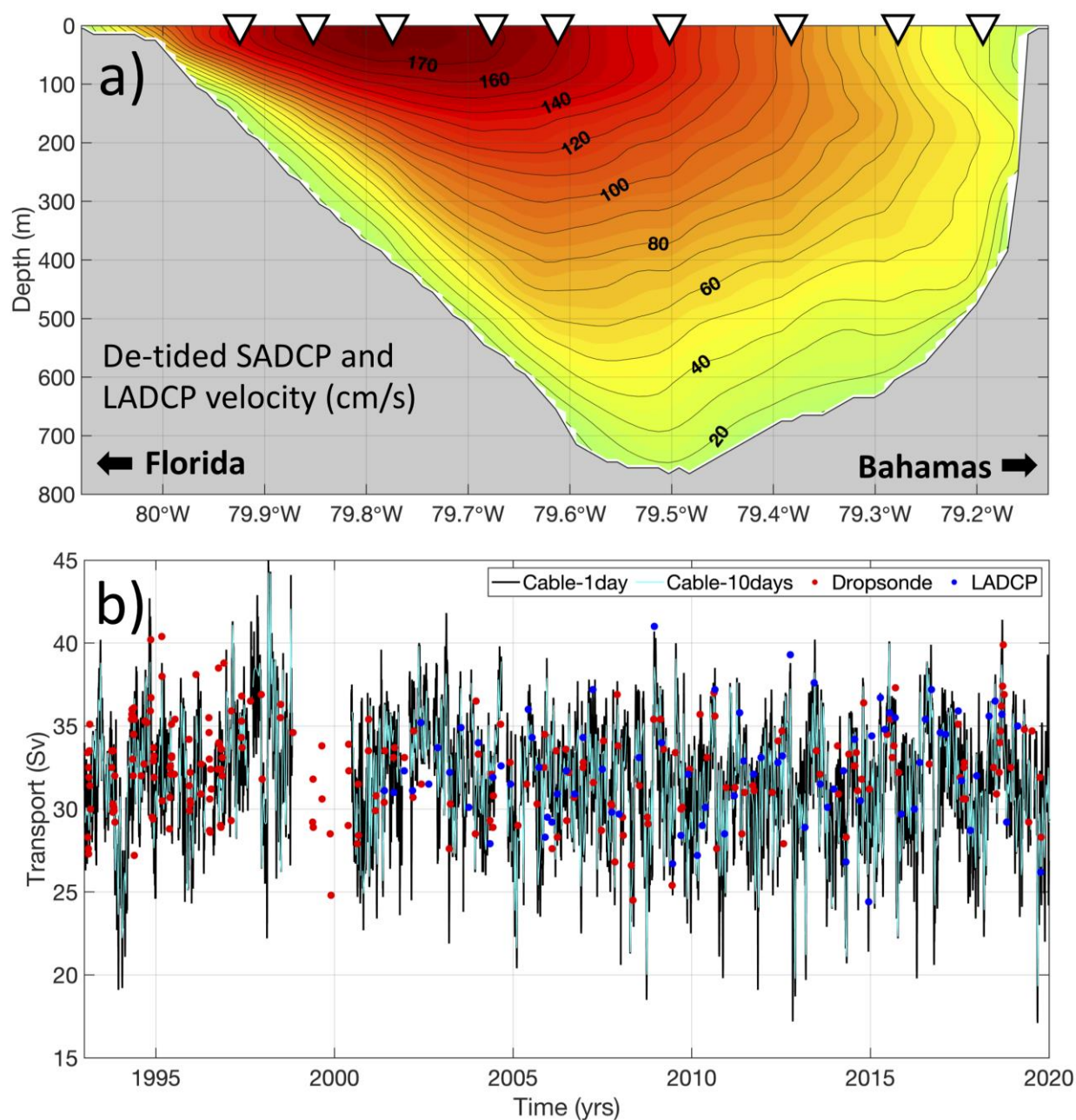


Figure 2. (a) Vertical section of meridional velocity obtained by merging underway ship ADCP (SADC) measurements and repeated lowered ADCP (LADCP) observations at the nine stations (shown by triangles) and averaged for 25 cruises between 2012 and 2018. (b) The Florida Current volume transport: (black) daily transport estimates, (cyan) transport estimates subsampled at 10-day intervals at the times of satellite overpasses, (red dots) transports measured with dropsonde floats, and (blue dots) transports measured with LADCP.

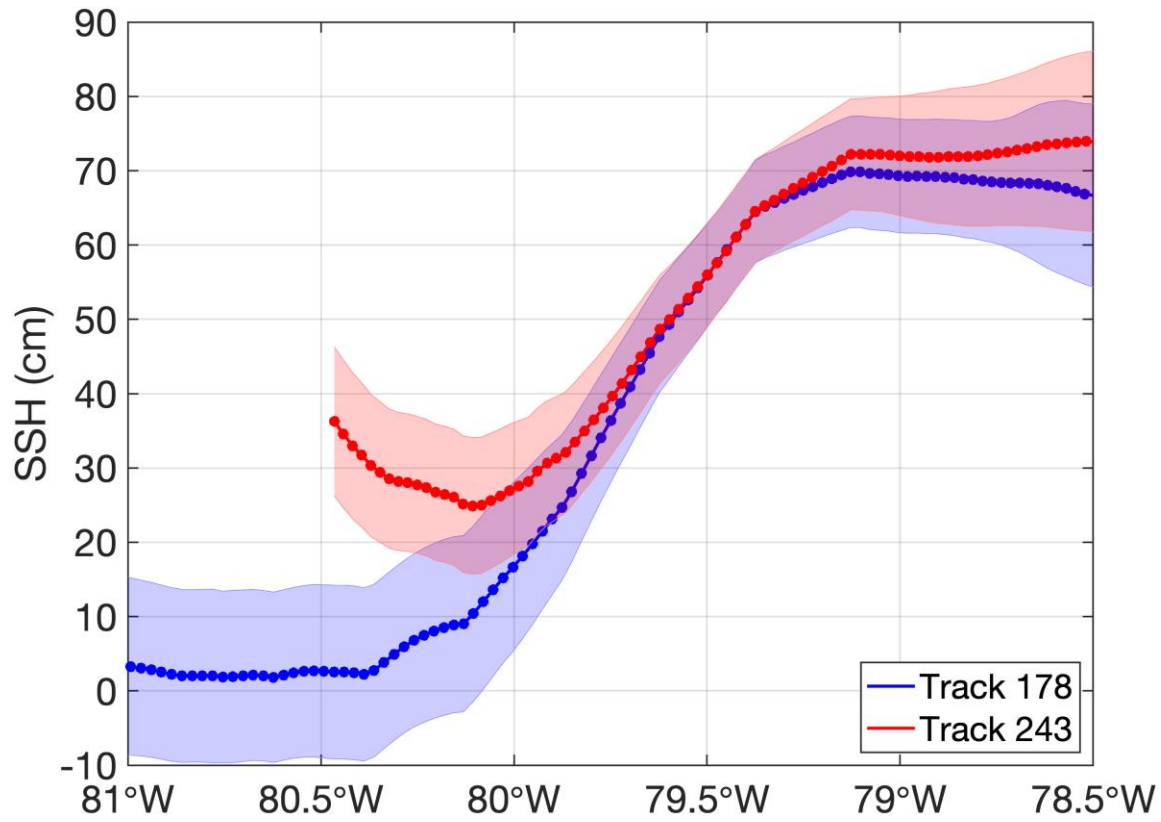


Figure 3. Sea surface height (SSH) along tracks 178 (blue) and 243 (red). The dotted curves show the time-mean SSH and shading denotes ± 1 standard deviation of the along-track SSH.

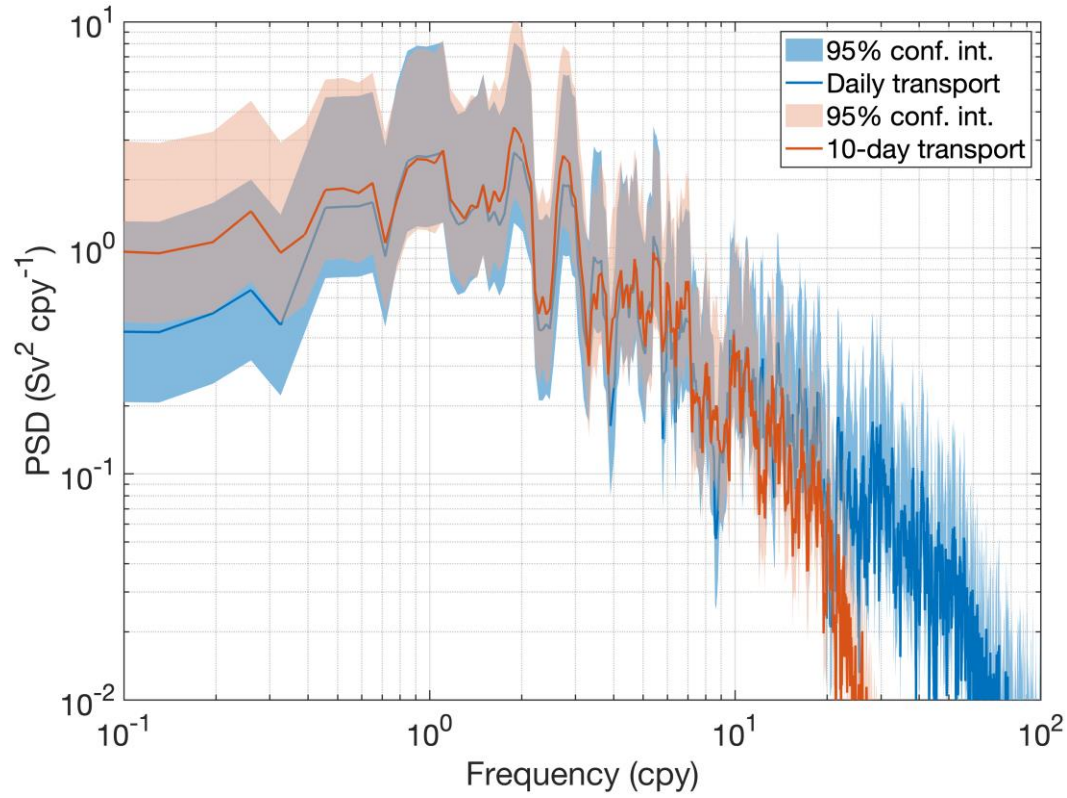


Figure 4. Frequency spectra of the fully-resolved daily cable transports (blue) and 10-day sampled cable transports (red). Shaded areas show the corresponding 95% confidence intervals.

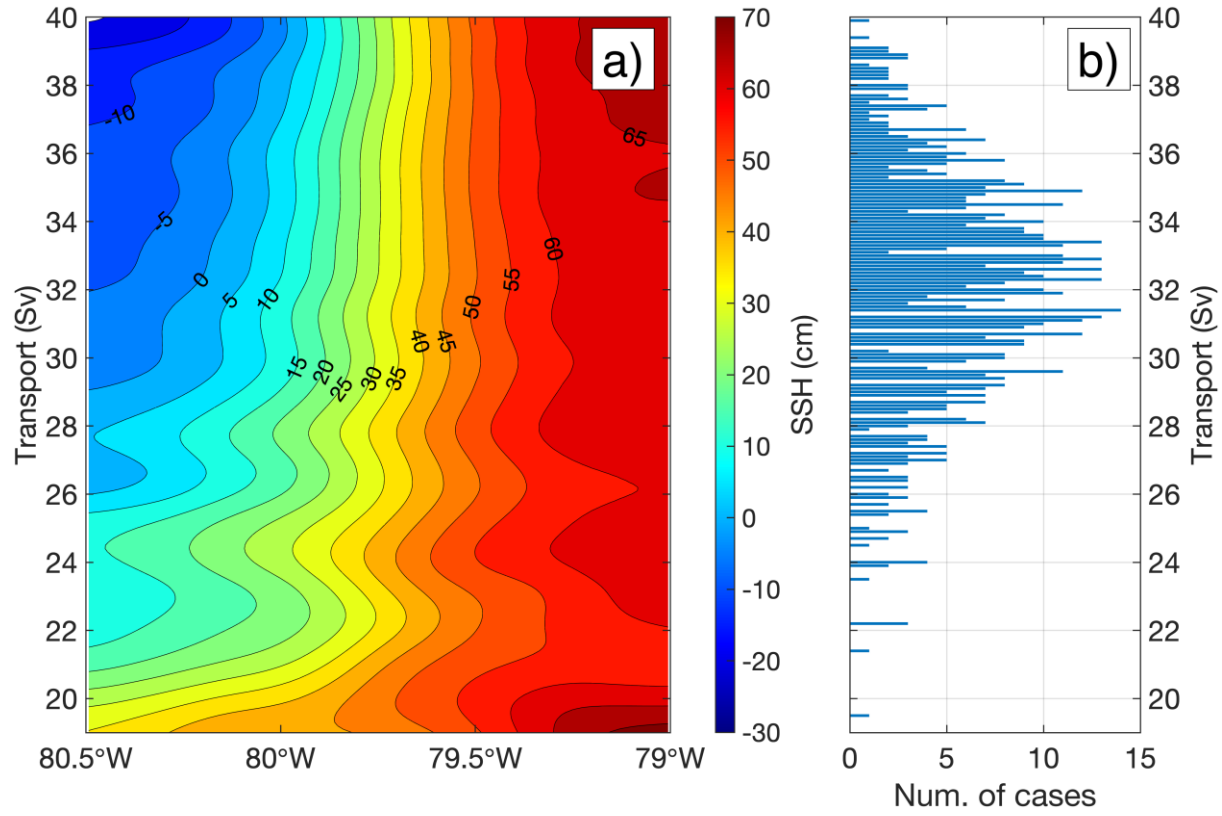


Figure 5. (a) Diagram showing the dependence of SSH along the track 178 on the FC volume transport and longitude; (b) histogram showing the number of existing SSH profiles per one transport value with a 0.1 Sv precision.

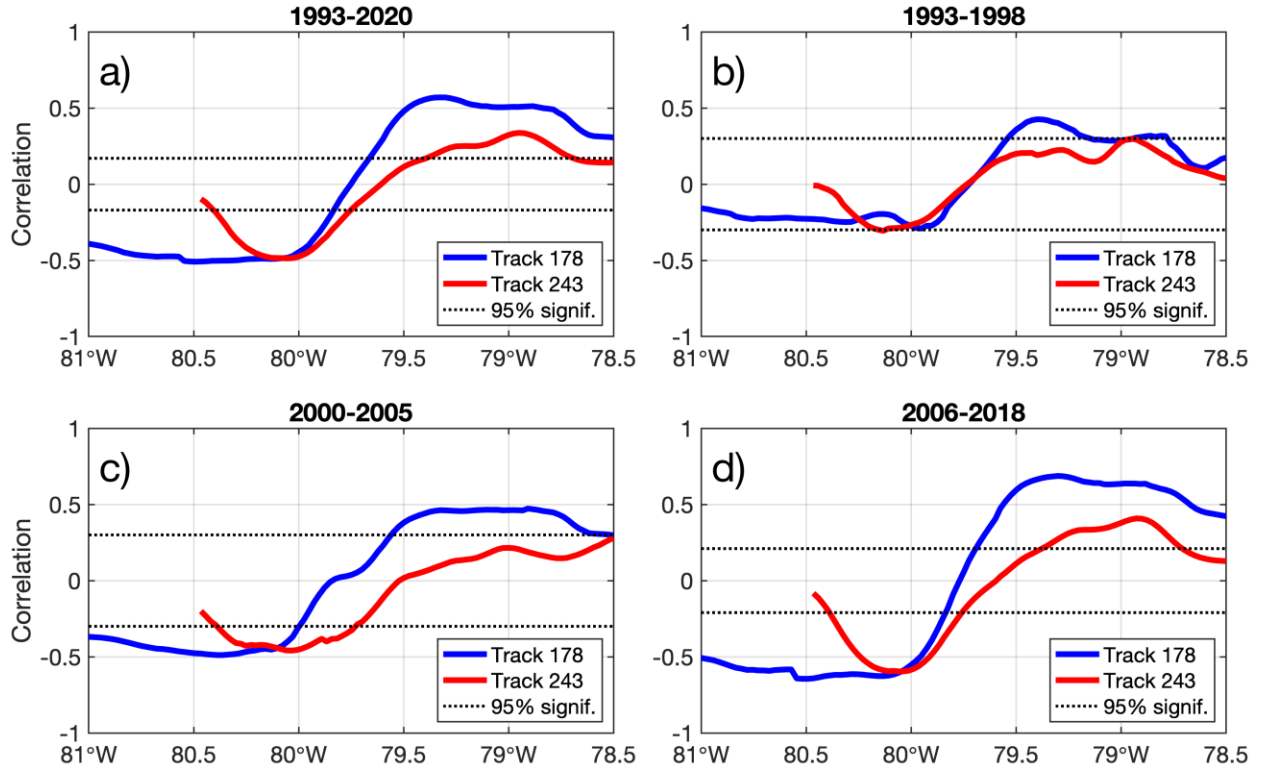


Figure 6. Correlation between the Florida Current volume transport (T_{Cable}) and the along-track SLA at tracks (blue) 178 and (red) 243 for different time intervals. The location of the tracks is shown in Fig. 1. The horizontal dotted lines show the 95% significance level for correlation.

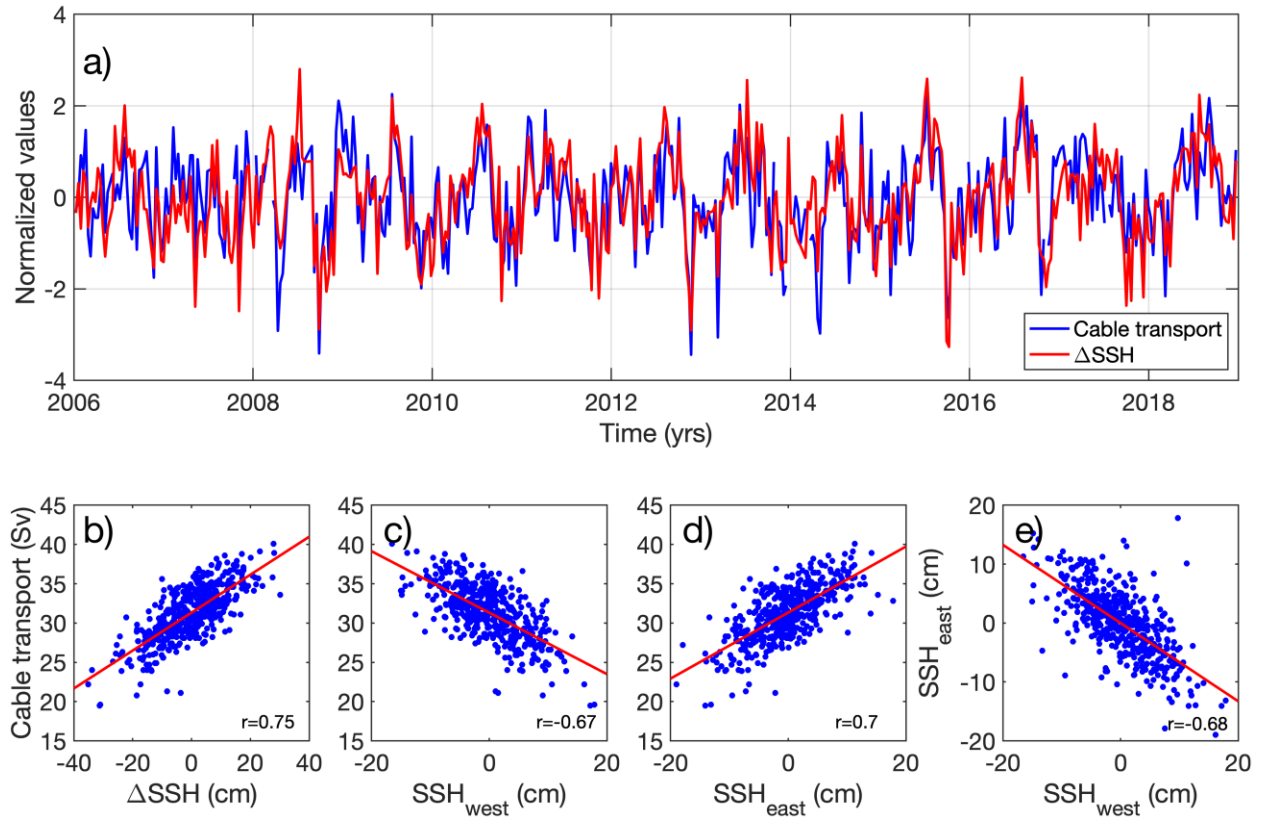


Figure 7. (a) Time series of the daily Florida Current volume transport from the submarine cable subsampled at the days of satellite overpasses (blue) and SSH differences (Δ SSH) between the western (79-79.5°W) and eastern (80-80.5°W) flanks of the Florida Current (red); the time series are normalized by subtracting the 2006-2018 mean and dividing by standard deviation. (b) Scatter plot of the SSH differences and the concurrent daily T_{FC} . (c) Scatter plot of the SSH averaged over the western flank of the FC (80-80.5°W) and the concurrent daily T_{FC} . (d) Scatter plot of the SSH averaged over the eastern flank of the FC (79-79.5°W) and the concurrent daily T_{FC} . (e) Scatter plot of the SSH averaged over the western flank of the FC (80-80.5°W) and over the eastern flank of the FC (79-79.5°W). Note that in order to make scatters centered around the zero SSH, the averages of Δ SSH, SSH_{west} , and SSH_{east} over the 2006-2018 period were subtracted from the respective variables.

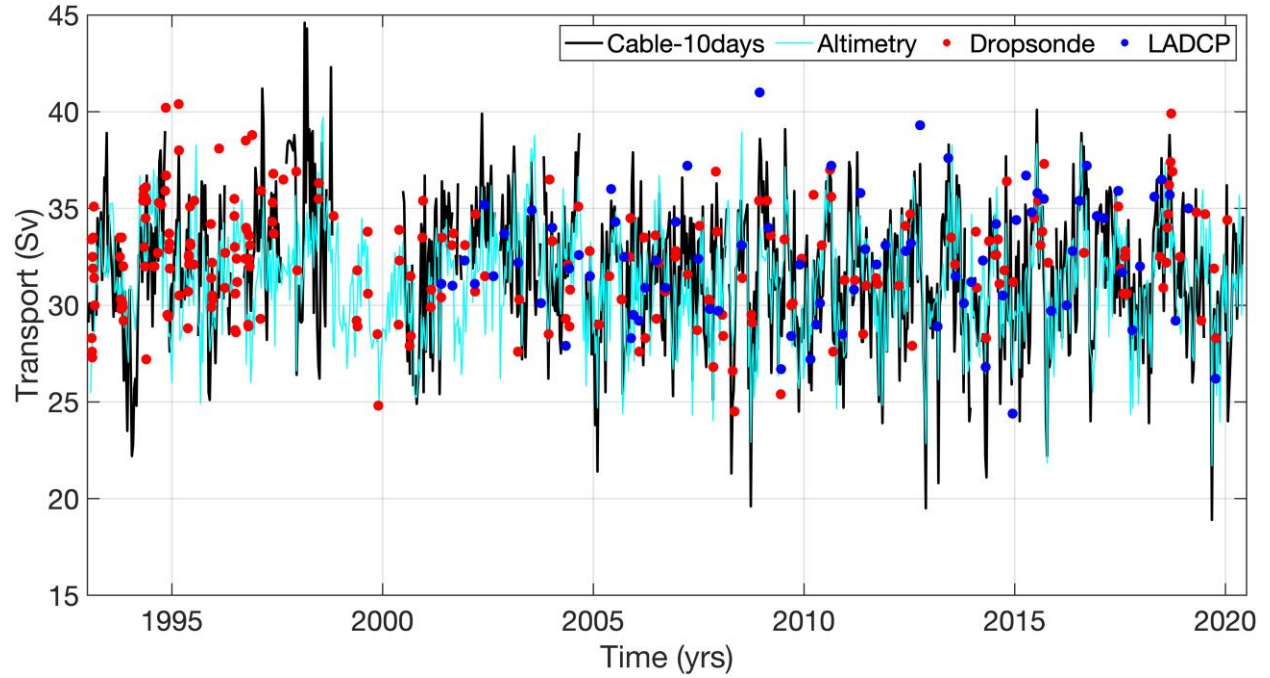


Figure 8. The Florida Current volume transport: cable transport estimates, T_{Cable} , subsampled at 10-day intervals at the times of satellite overpasses (black), altimetry-derived transport estimates, $T_{\text{Altimetry}}$ (cyan), transports measured with dropsonde floats, $T_{\text{Dropsonde}}$ (red dots), and transports measured with LADCP, T_{LADCP} (blue dots).

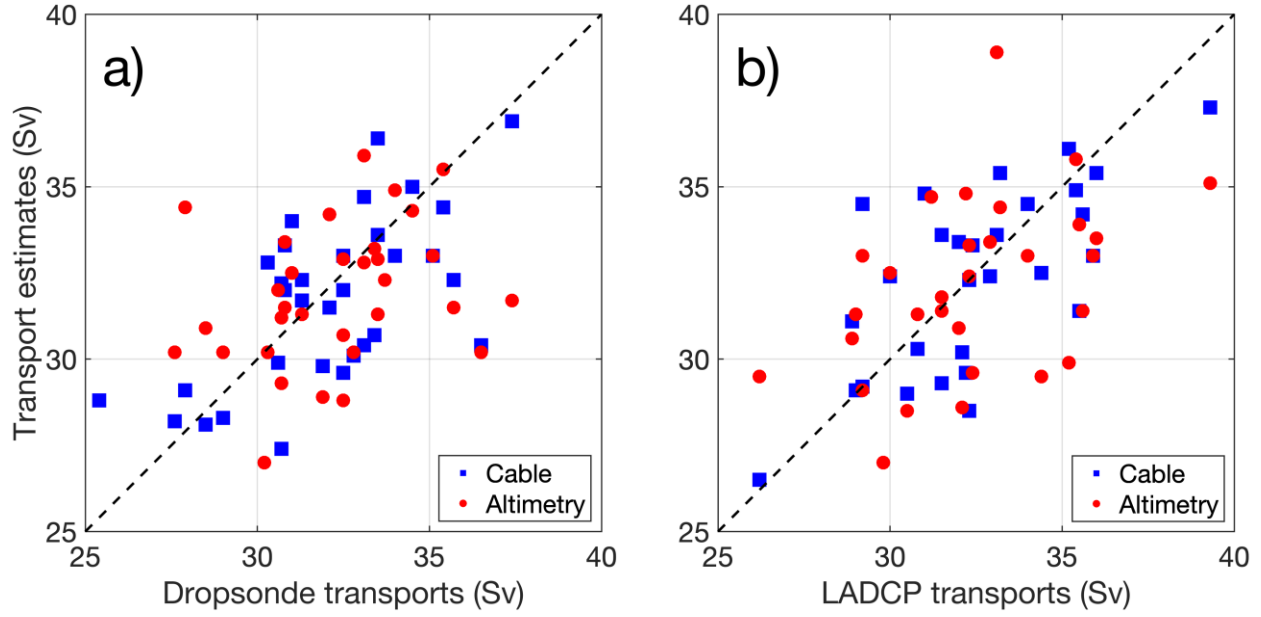


Figure 9. Comparison between the direct measurements of the FC volume transport with (a) dropsonde and (b) LADCP sections and the estimates of the FC volume transport from the voltages measured on the submarine cable (blue squares) and from SSH differences measured by satellite altimetry (red circles). A total of 32 dropsonde and 30 LADCP sections over the period of 2001-2019 were used for the comparison.

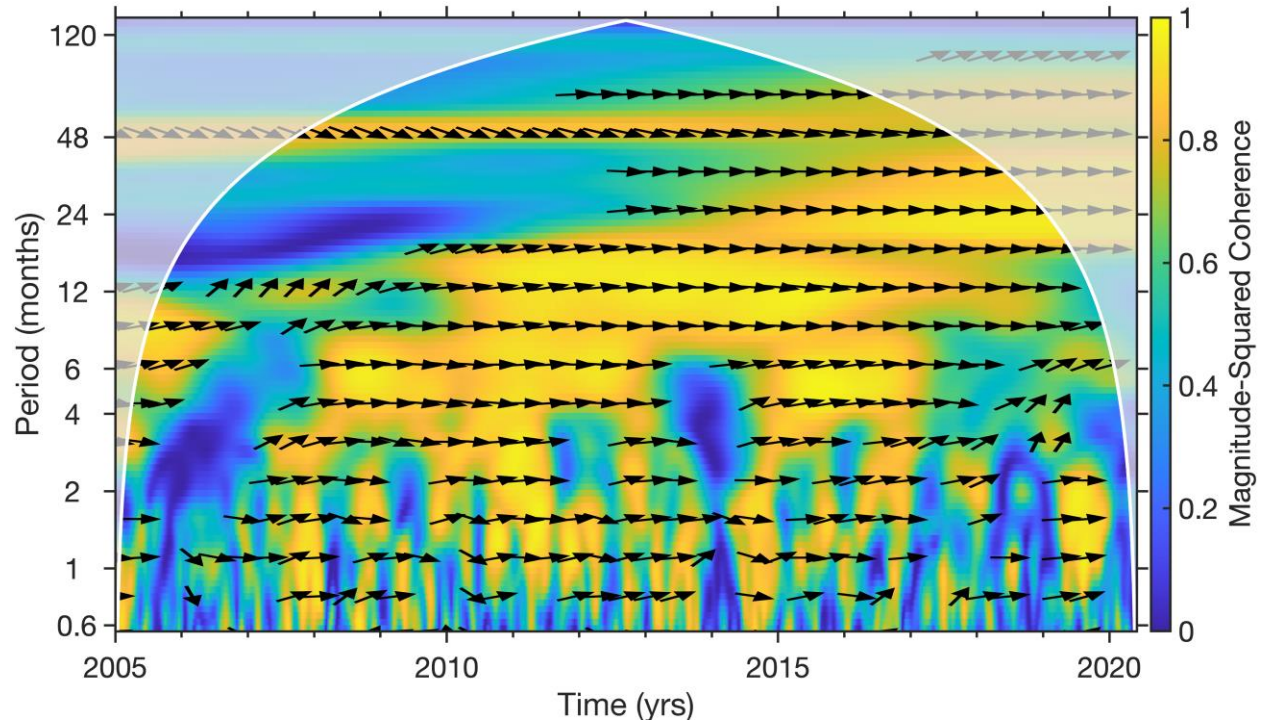


Figure 10. The magnitude-squared wavelet coherence between the cable- and altimetry-derived FC transport estimates. The direction of the arrows in the coherence plot corresponds to the phase lag on the unit circle, with the forward direction indicating an in-phase relationship. Frequency is plotted on a logarithmic scale. The cone of influence in the coherence plot (blurred area) indicates where edge effects occur in the coherence data.

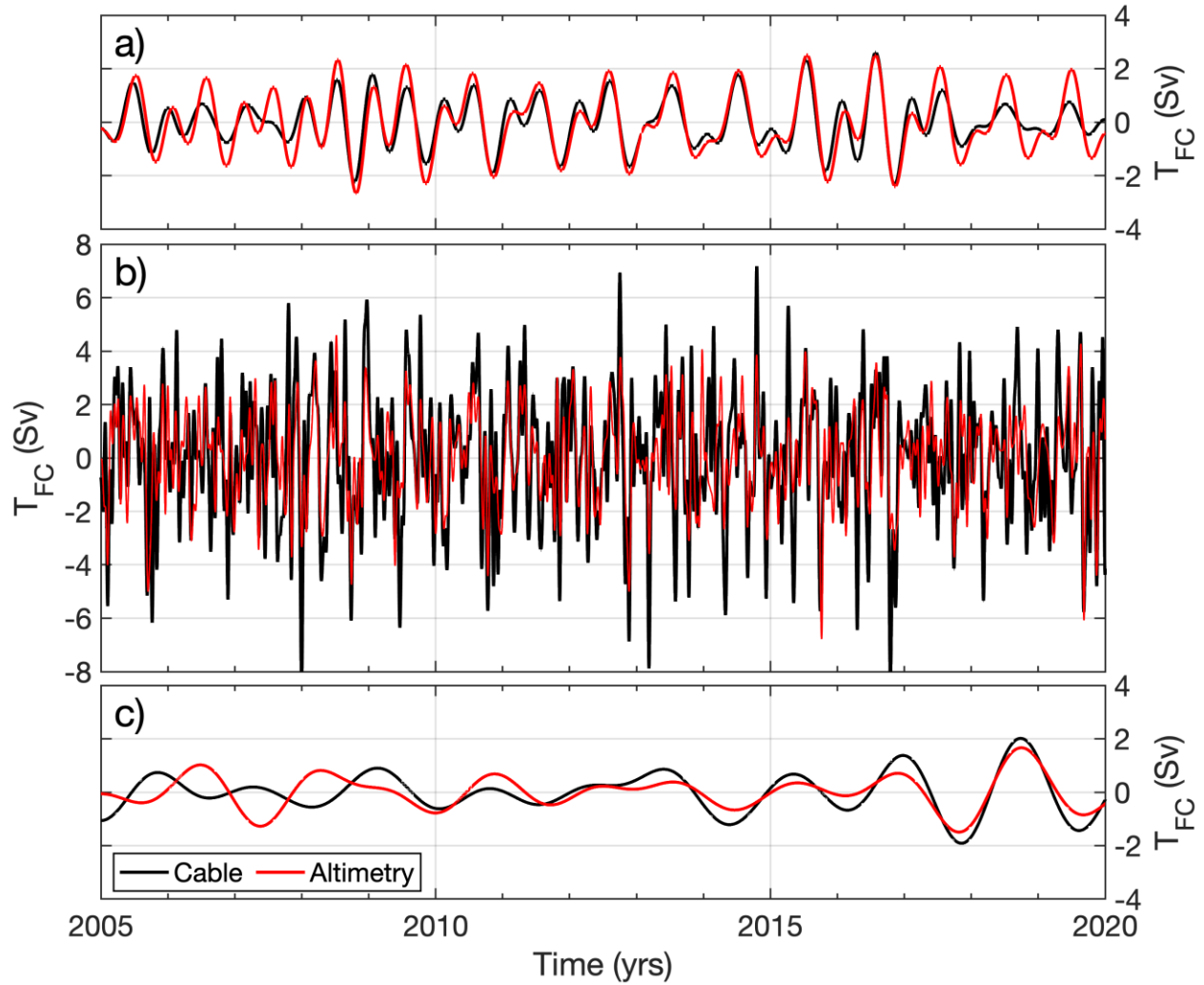


Figure 11. The FC volume transport anomalies, reconstructed by inverting the continuous wavelet transforms of (black curves) T_{Cable} and (red curves) $T_{Altimetry}$ over the range of periods associated with the following signals: (a) the seasonal cycle, obtained by summing up the annual (periods from 345 to 385 days) and semi-annual (periods from 170 to 195 days) cycles; (b) the intra-seasonal variability (periods from 20 to 385 days) with the seasonal cycle subtracted, and (c) the inter-annual variability (periods longer than 540 days).

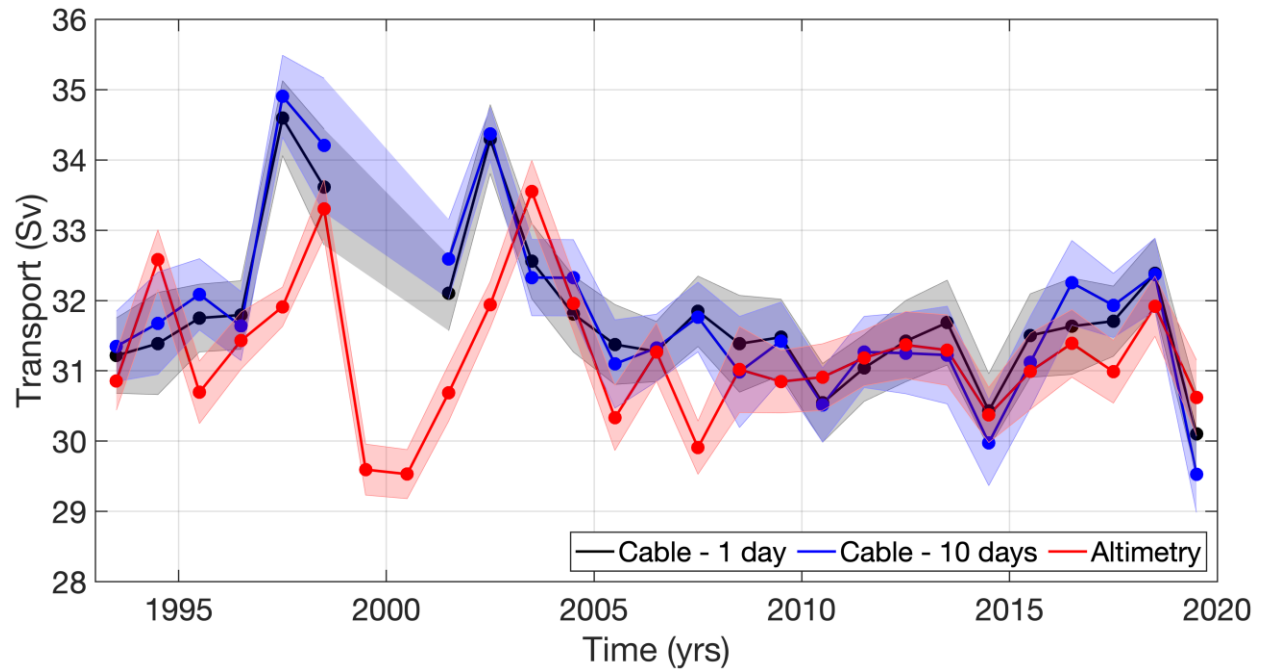


Figure 12. Yearly averages of the (black) daily and (blue) 10-day sampled T_{Cable} , and (red) $T_{\text{Altimetry}}$. Shaded areas show ± 1 standard error for each estimate.

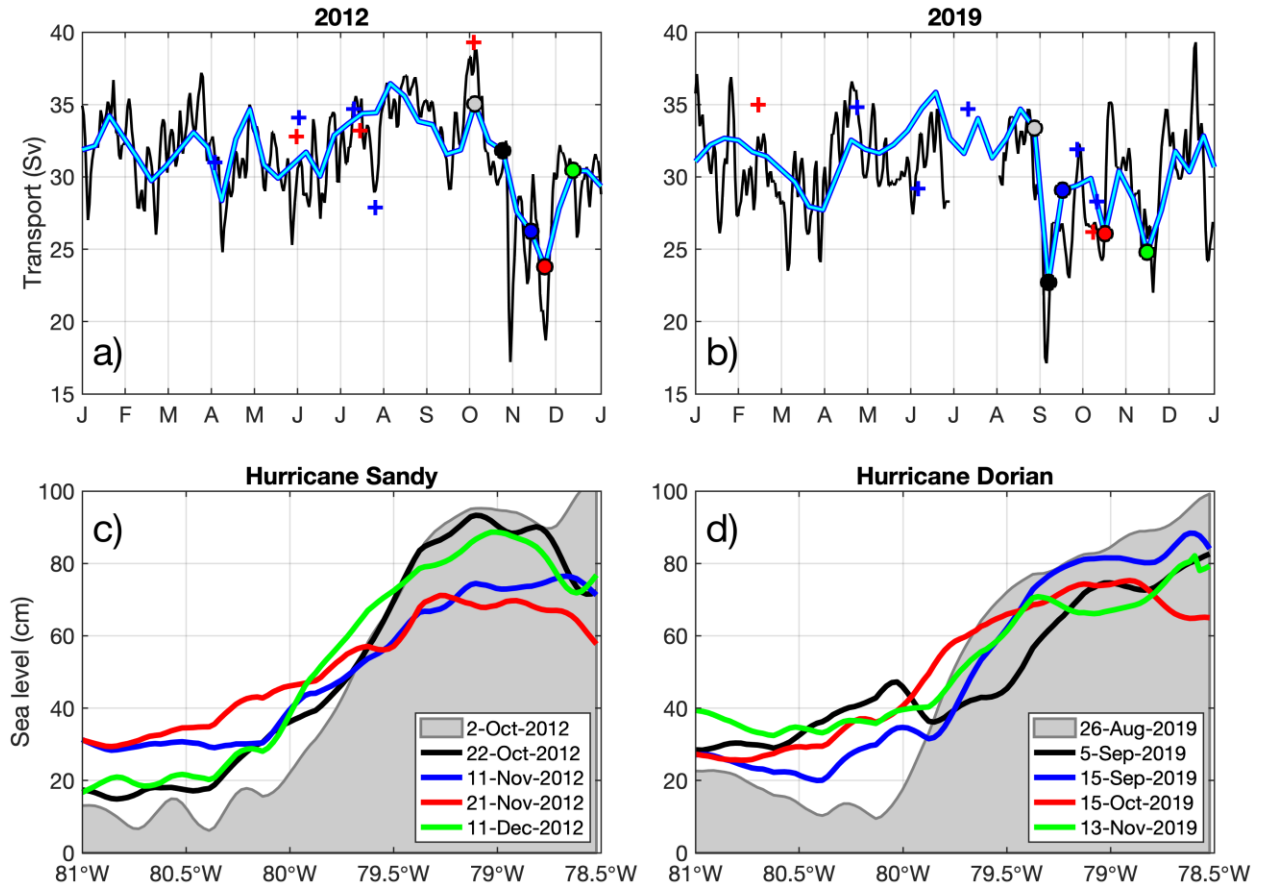


Figure 13. (a-b) The FC volume transport estimates from the cable voltages (black curves), altimetry (cyan curves), dropsonde measurements (red crosses), and LADCP measurements (blue crosses) in 2012 and 2019. Hurricane Sandy was passing over the Straits of Florida on Oct. 25-30, 2012, and Hurricane Dorian was affecting the Straits of Florida on Sep. 1-6, 2019. (c-d) SSH along the track 178 around the times when (c) Hurricane Sandy and (d) Hurricane Dorian were passing over the Straits of Florida. The along-track SSH profiles shown in (c) and (d) correspond to volume transport values shown by circles in (a) and (b) highlighted by the same color.

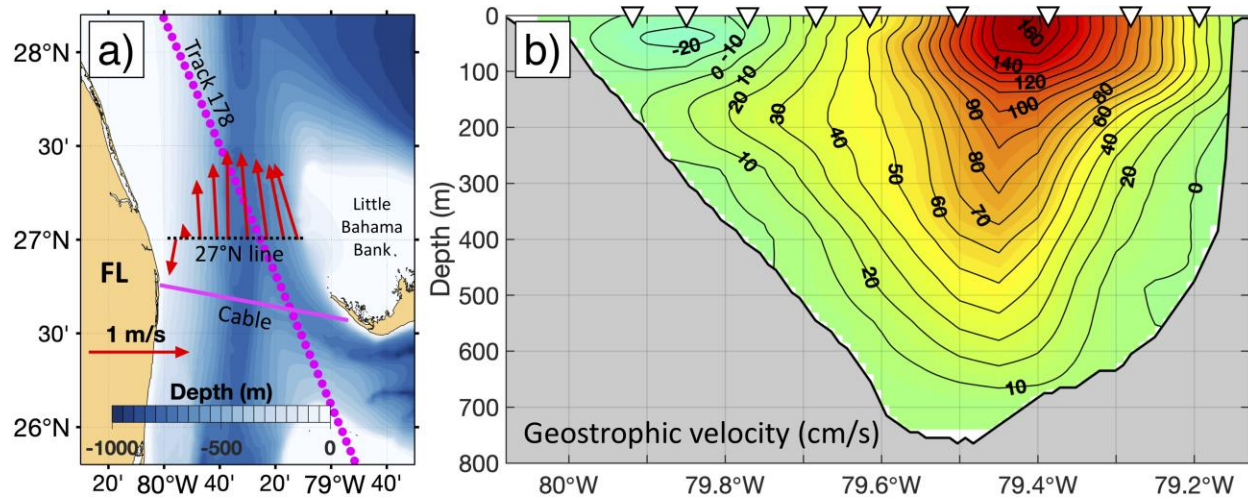


Figure 14. The Florida Current velocities at 27°N observed during a dropsonde/XBT cruise on September 6, 2019: (a) the depth-integrated velocities (red arrows) at nine stations along the 27°N line derived from the dropsonde measurements; (b) the northward geostrophic velocity (cm/s) calculated from temperature and salinity profiles at nine stations (triangles) along the 27°N line; temperature profiles were directly measured with XBTs and salinity profiles were derived from an empirical relationship between temperature and salinity at each station. Note an unusual southward flow near Florida coast and an eastward shift of the Florida Current jet (compare to the mean state shown in Fig. 2a).

Table 1. Abbreviations of the FC volume transport used throughout the manuscript.

Abbreviation	Description
T_{FC}	True Florida Current volume transport
T_{Cable}	Inferred from voltages on the submarine cable
$T_{Dropsonde}$	Directly measured with dropsondes during cruises along 27°N
T_{LADCP}	Directly measured with LADCP during cruises along 27°N
T_{BPR}	Inferred from bottom pressure differences
$T_{Altimetry}$	Inferred from satellite altimetry measurements

Table 2. Accuracies of the Florida Current volume transport estimates from different observing platforms.

	Type of the FC volume transport estimate, T_{FC}						
	$T_{Dropsonde}$ (Garcia et al., 2014)	T_{LADCP} (Garcia et al., 2014)	T_{BPR} (Meinen et al., 2020)	T_{Cable}	$T_{Altimetry}$		
					Compared to T_{Cable}	Compared to $T_{Dropsonde}$	Compared to T_{LADCP}
Accuracy, ϵ (Sv)	0.8	1.3	2.7	1.5	2.1	2.0	1.9

Table 3. Statistics of comparisons between direct measurements of T_{FC} with dropsondes ($T_{Dropsonde}$) and LADCP (T_{LADCP}) and quasi-concurrent estimates of T_{FC} from the cable (T_{Cable}) and the along-track satellite altimetry ($T_{Altimetry}$) in 2001-2019, excluding the dropsonde sections used for cable calibration. The direct measurements used for the comparison were taken during the ± 48 -hour windows around the times of satellite overpasses across the FC along track 178.

Type of T_{FC} measurement during ship sections at 27°N	Number of collocated ship sections at 27°N	Comparison to 10-day subsampled cable transport estimates, T_{Cable}		Comparison to altimetry-derived transport estimates, $T_{Altimetry}$	
		Correlation coefficient, r	RMS difference, ϵ_{total}^* (Sv)	Correlation coefficient, r	RMS difference, ϵ_{total}^* (Sv)
$T_{Dropsonde}$	32	0.63	2.2	0.29	2.7
T_{LADCP}	30	0.68	2.2	0.44	2.8

Table 4. Quantifying statistics of the comparison between T_{Cable} and $T_{\text{Altimetry}}$ signals reconstructed by inverting the inverse continuous wavelet transforms for the seasonal (annual + semi-annual), intra-seasonal, and inter-annual time scales.

Time scales of the variability		Seasonal	Annual	Semi-annual	Intra-seasonal	Inter-annual
Periods used to invert the continuous wavelet transform (days)		170-195 345-385	345-385	170-195	20-170 195-345	>540
$r(T_{\text{Cable}}, T_{\text{Altimetry}})$		0.90	0.93	0.91	0.67	0.67
RMS ($T_{\text{Cable}} - T_{\text{Altimetry}}$) (Sv)		0.5	0.4	0.3	1.8	0.6
Standard deviation of the signal (Sv)	Cable	0.9	0.5	0.7	2.4	0.7
	Altimetry	1.1	0.8	0.8	1.7	0.6

Table 5. The FC volume transport estimates from cable voltage (T_{Cable}) and satellite altimetry ($T_{\text{Altimetry}}$) on the dates around the passages of Hurricane Sandy in 2012 and Hurricane Dorian in 2019 over the Straits of Florida.

Date	2012					2019				
	2-Oct	22-Oct	11-Nov	21-Nov	11-Dec	26-Aug	5-Sep	15-Sep	15-Oct	13-Nov
T_{Cable} (Sv)	37.3	30.3	25.3	19.5	30.6	29.2	18.9	26.8	26.6	27.0
$T_{\text{Altimetry}}$ (Sv)	35.1	31.6	25.5	22.8	30.1	33.3	21.7	28.6	25.3	24.0

Figure 1.

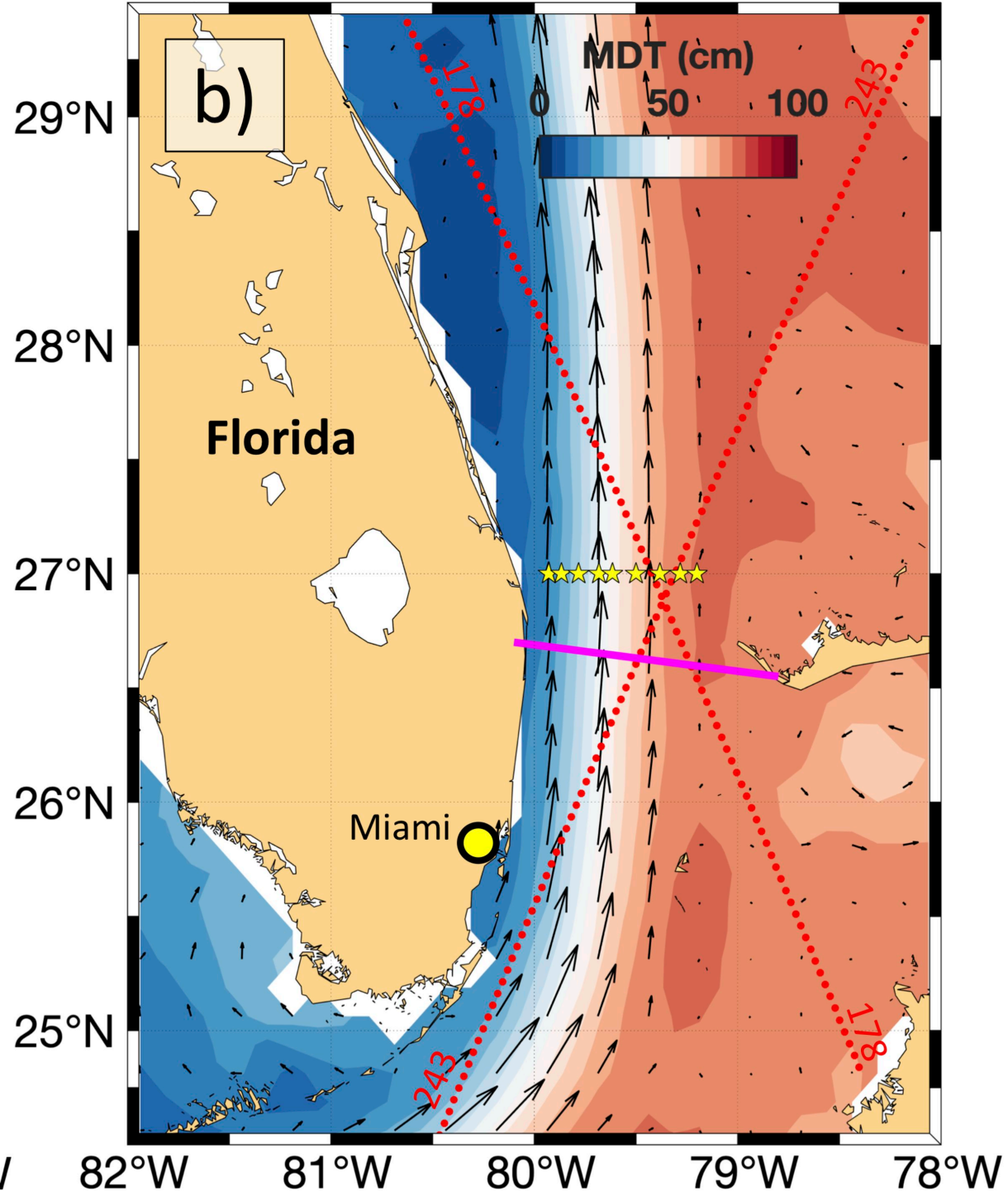
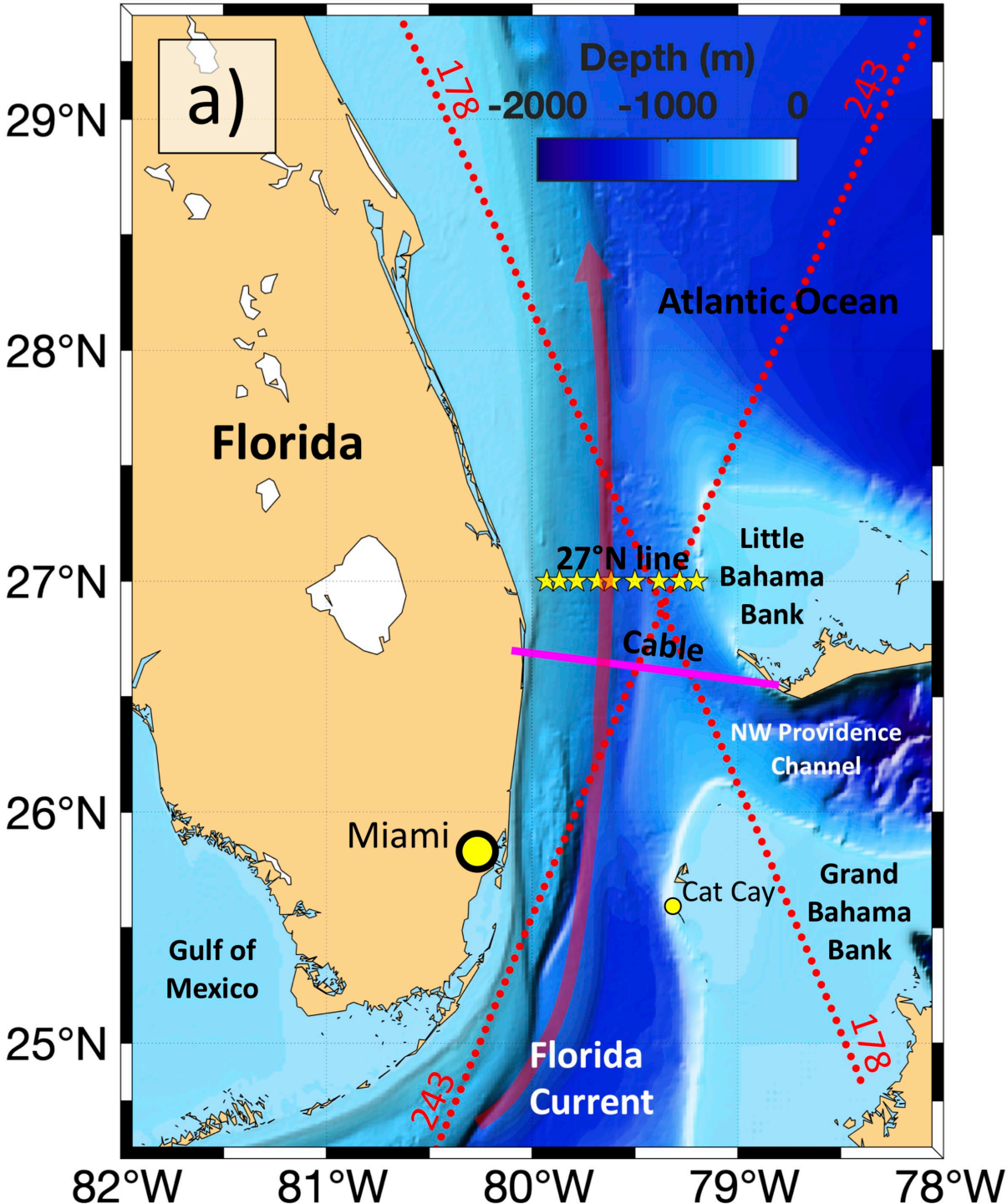


Figure 2.

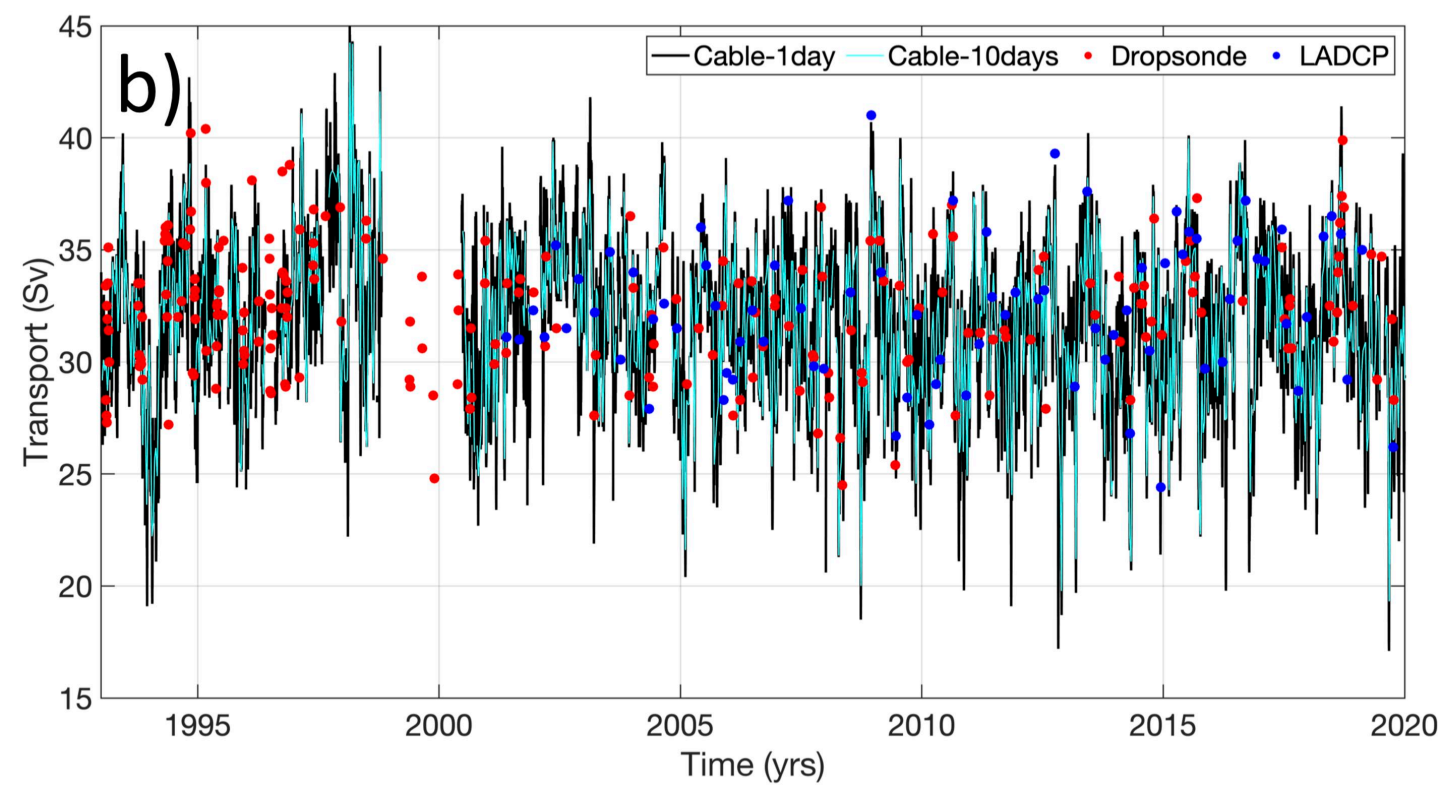
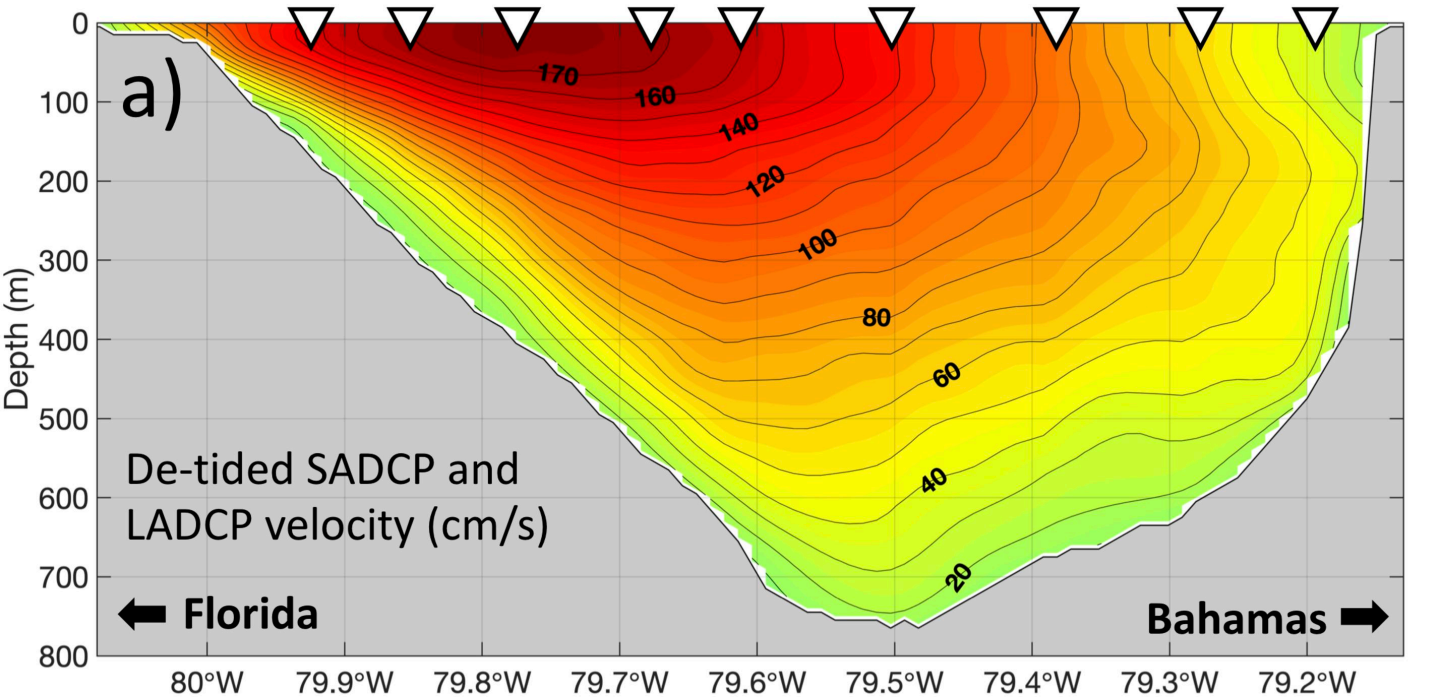


Figure 3.

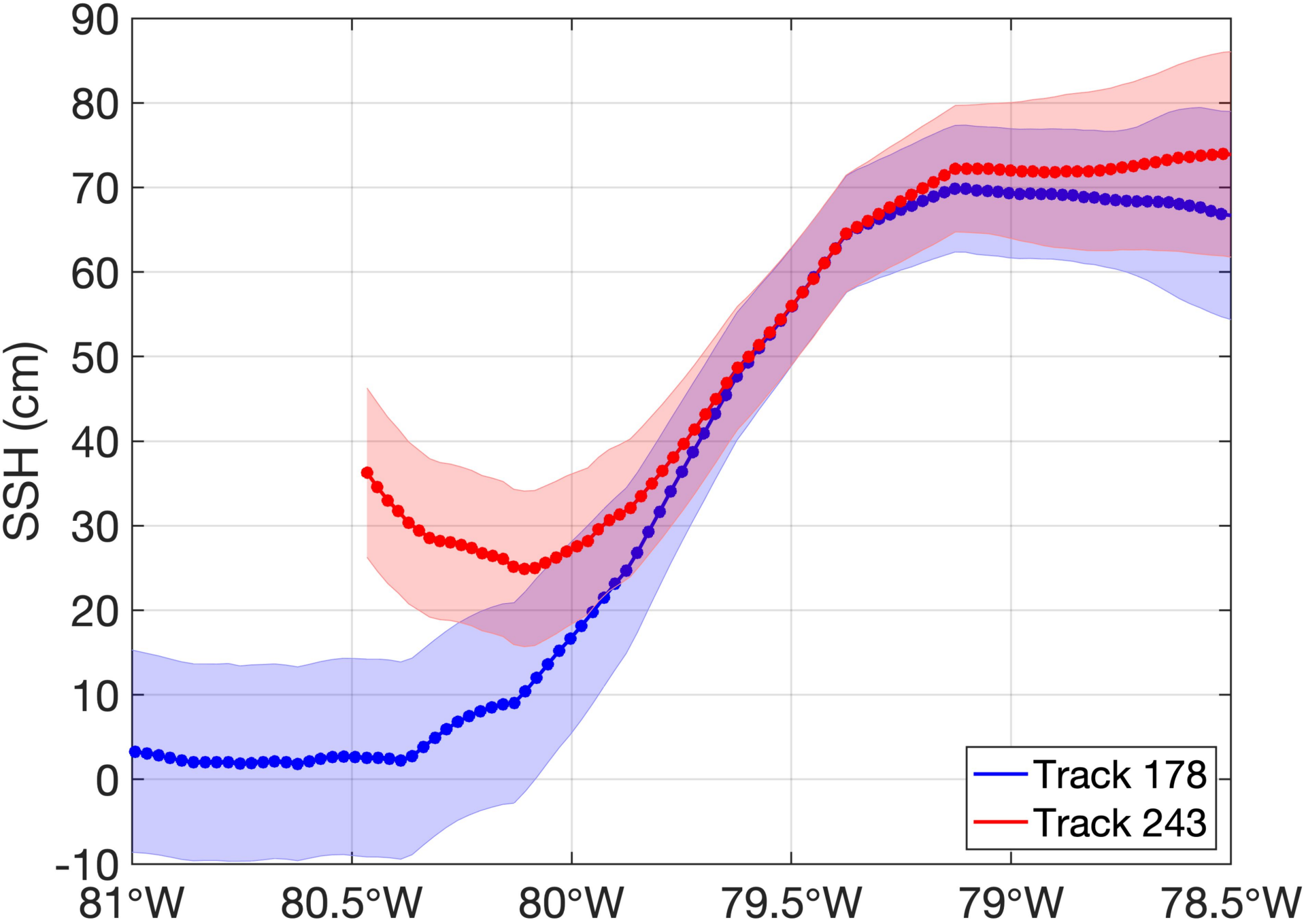


Figure 4.

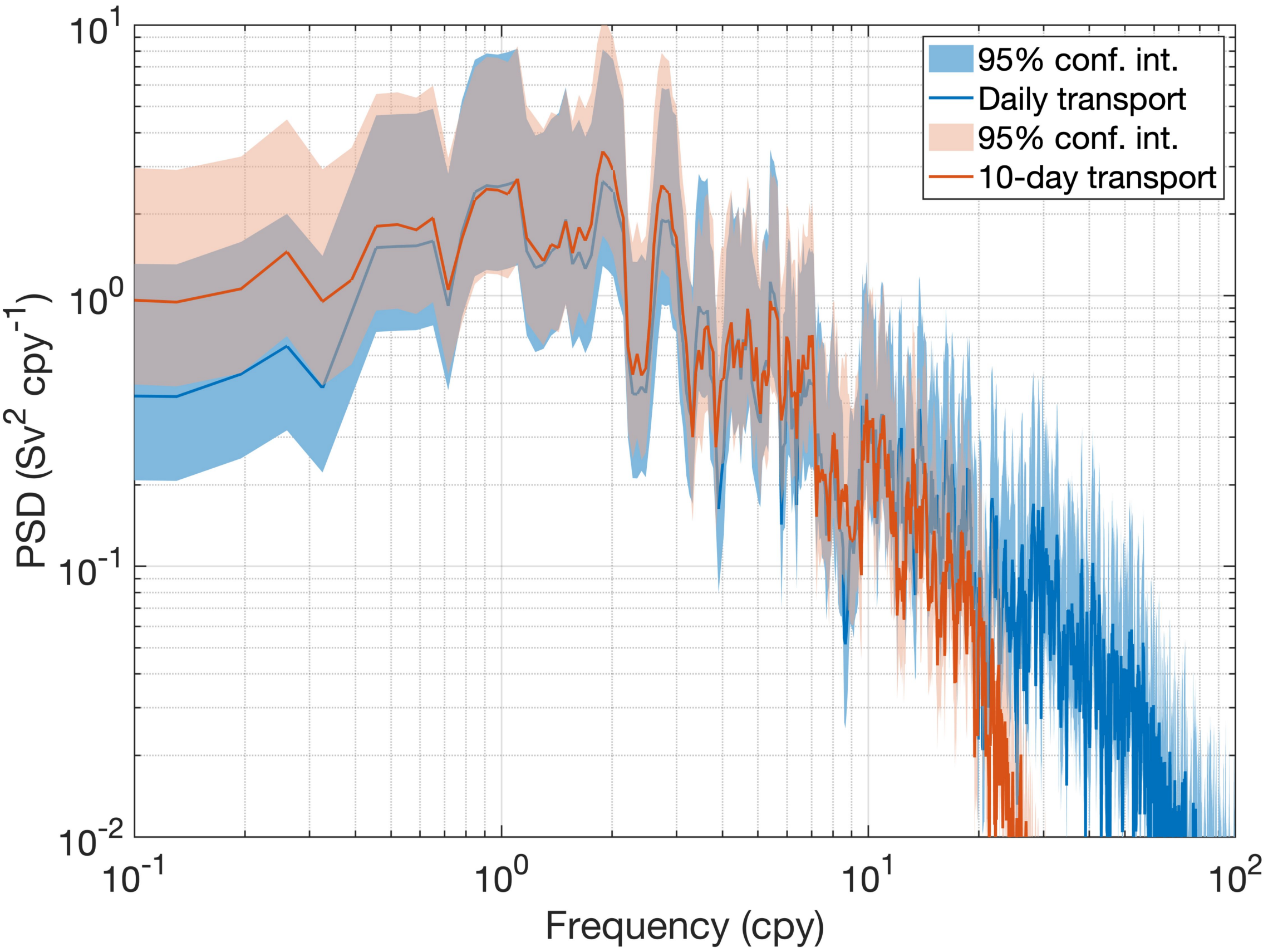


Figure 5.

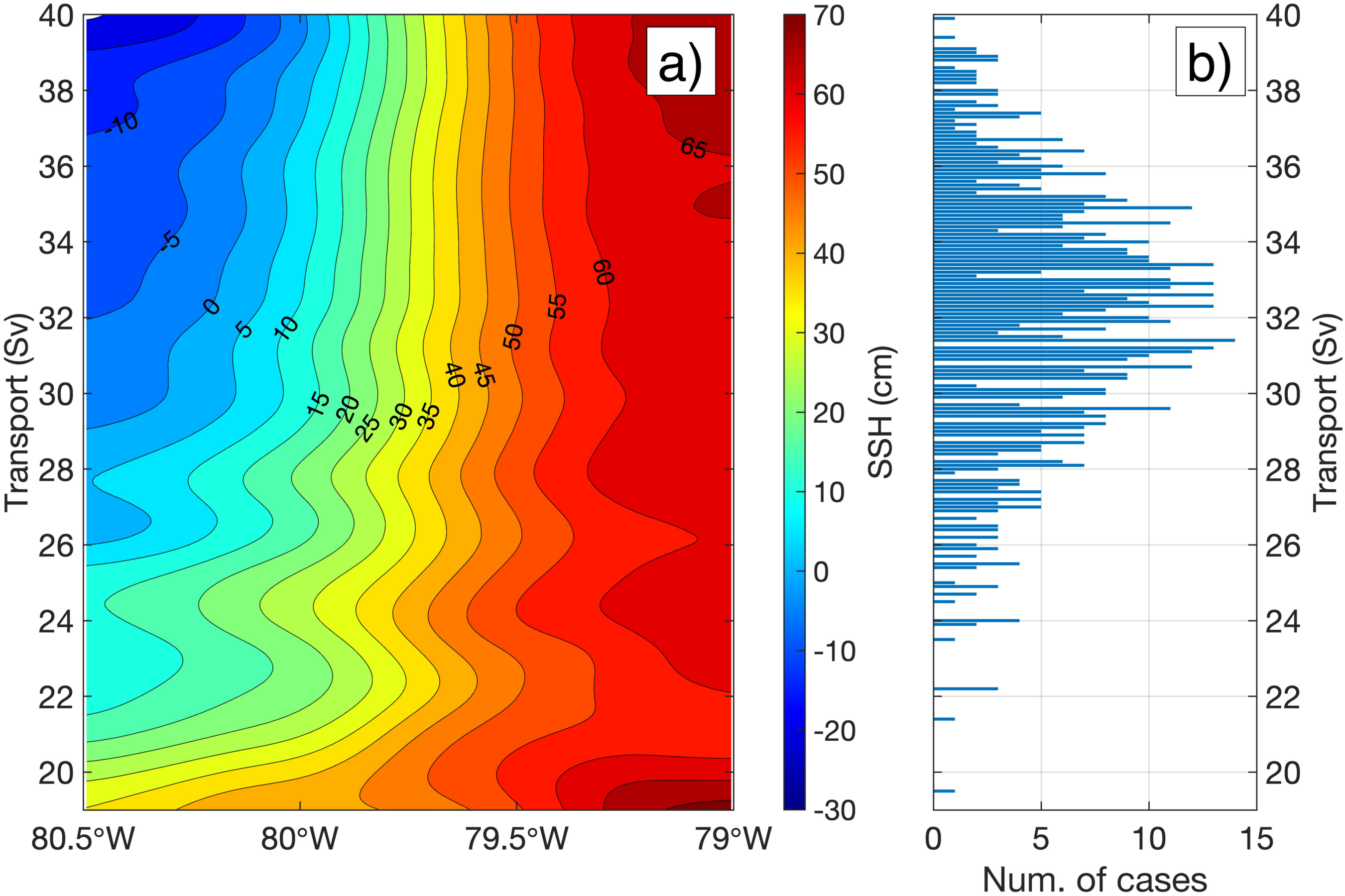


Figure 6.

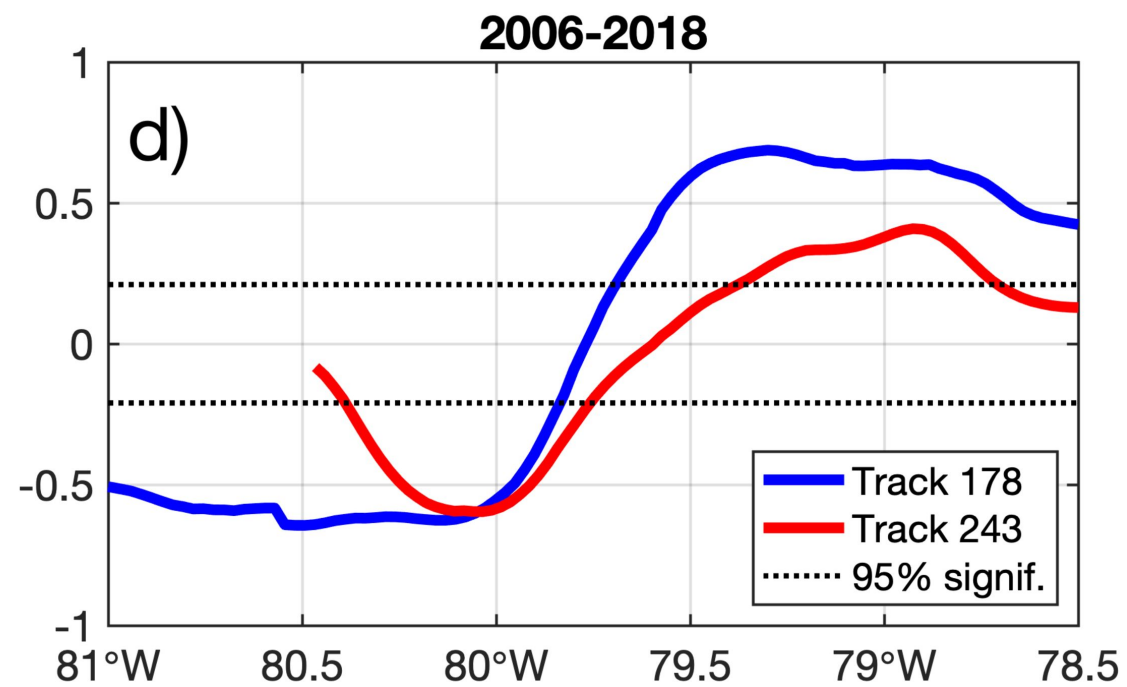
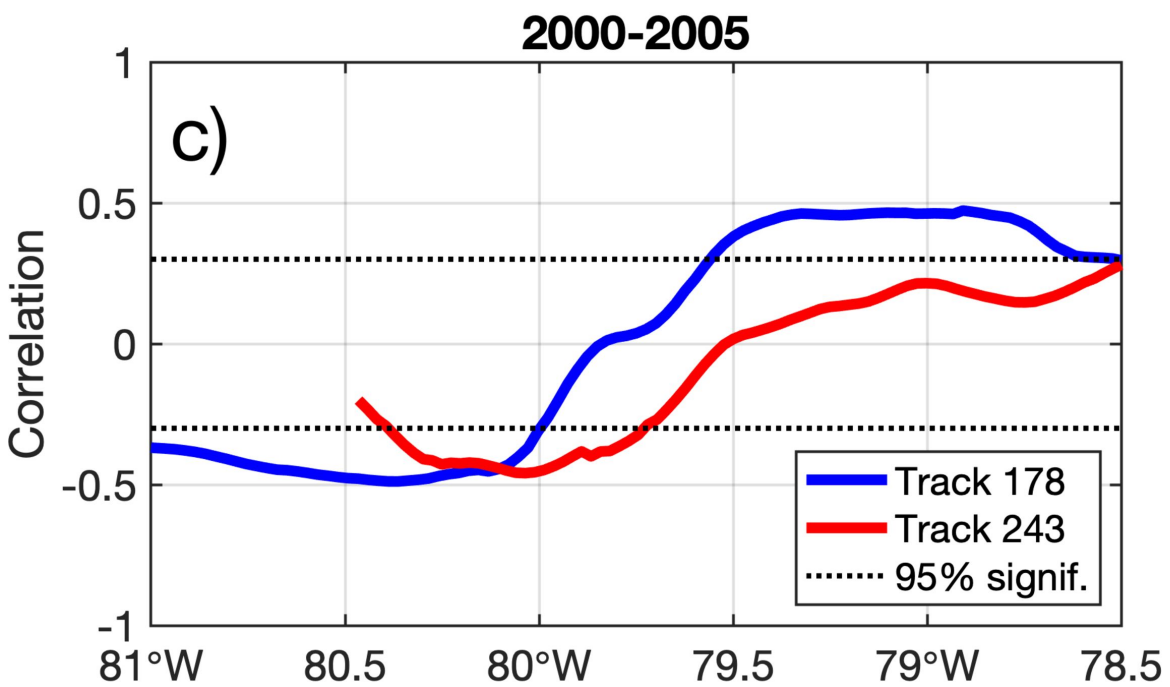
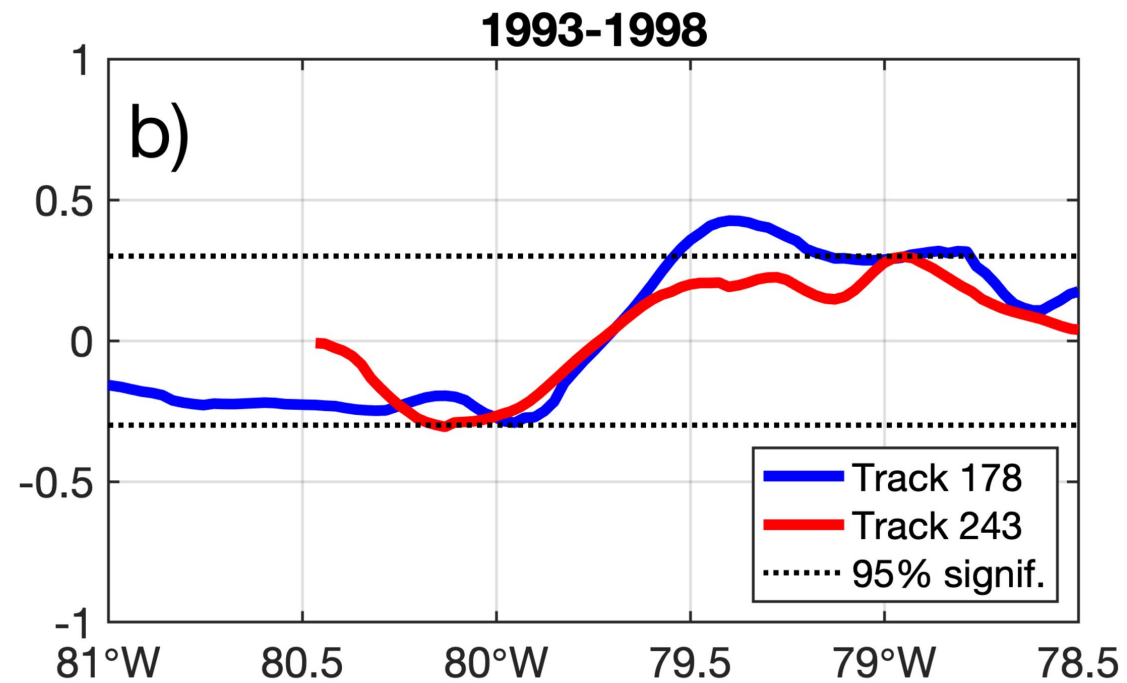
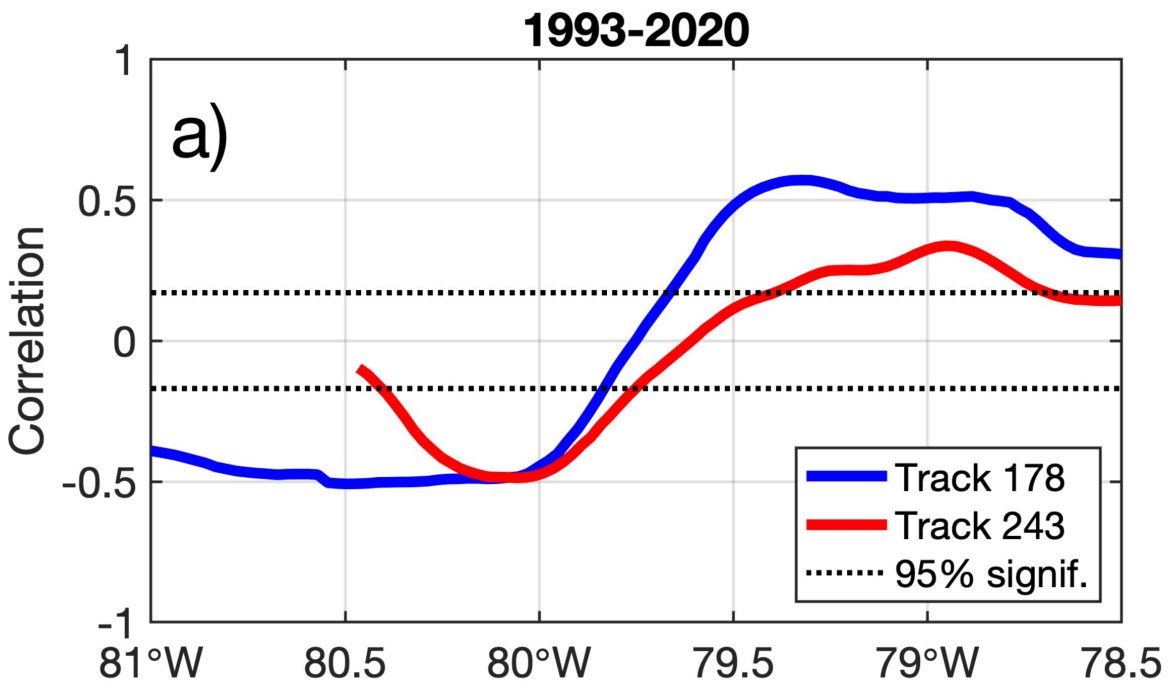


Figure 7.

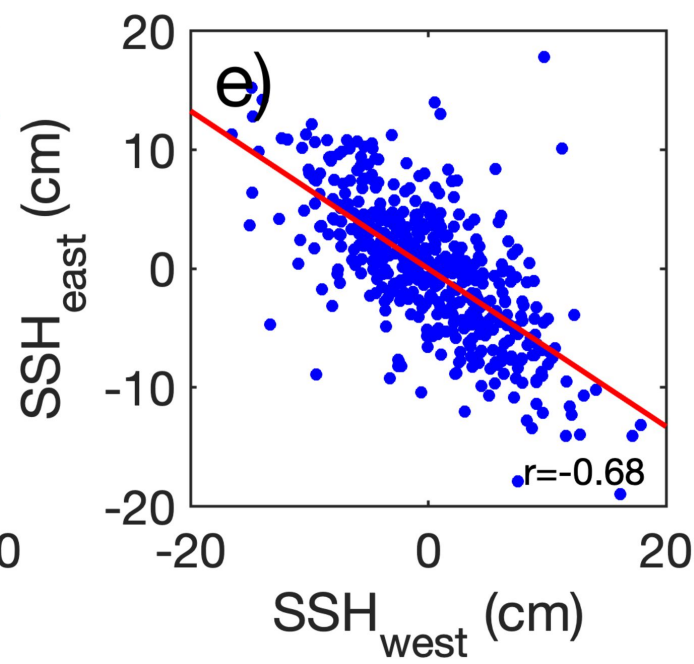
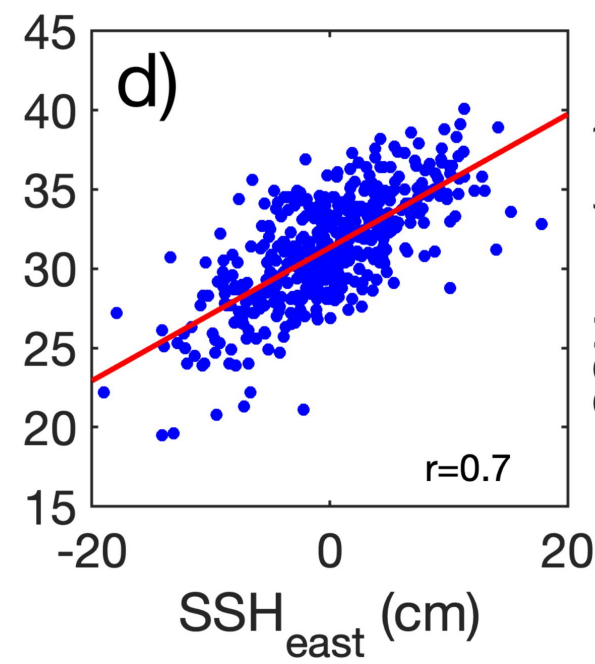
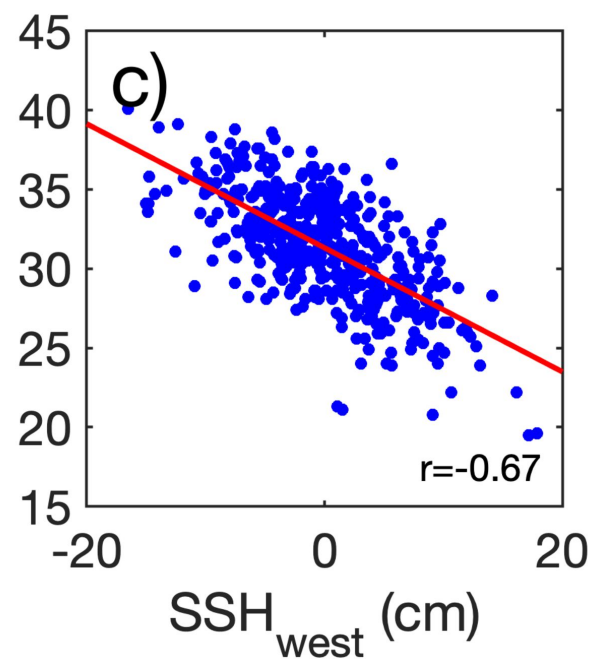
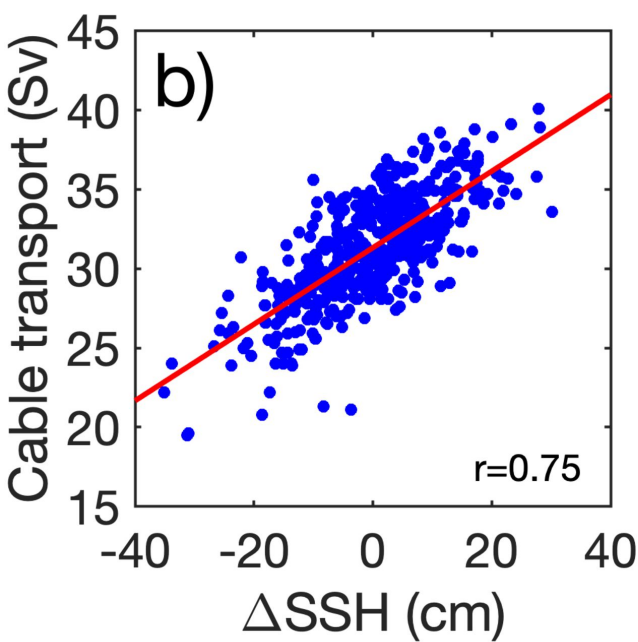
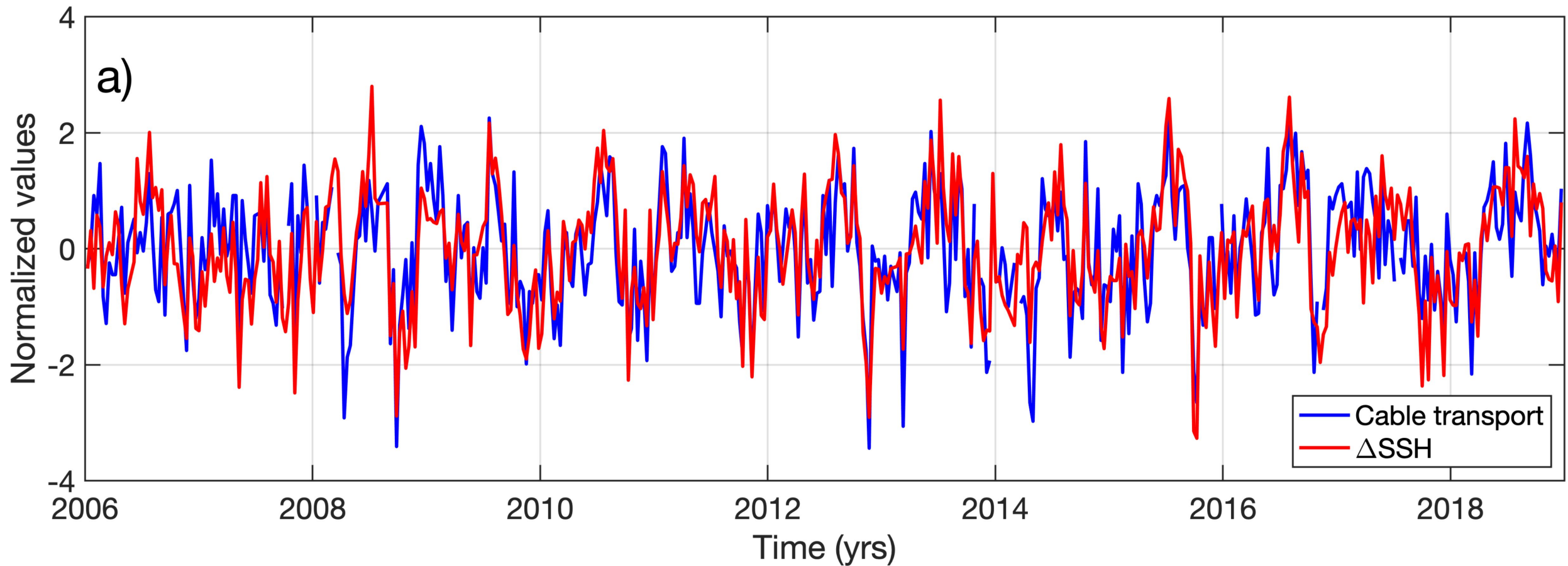


Figure 8.

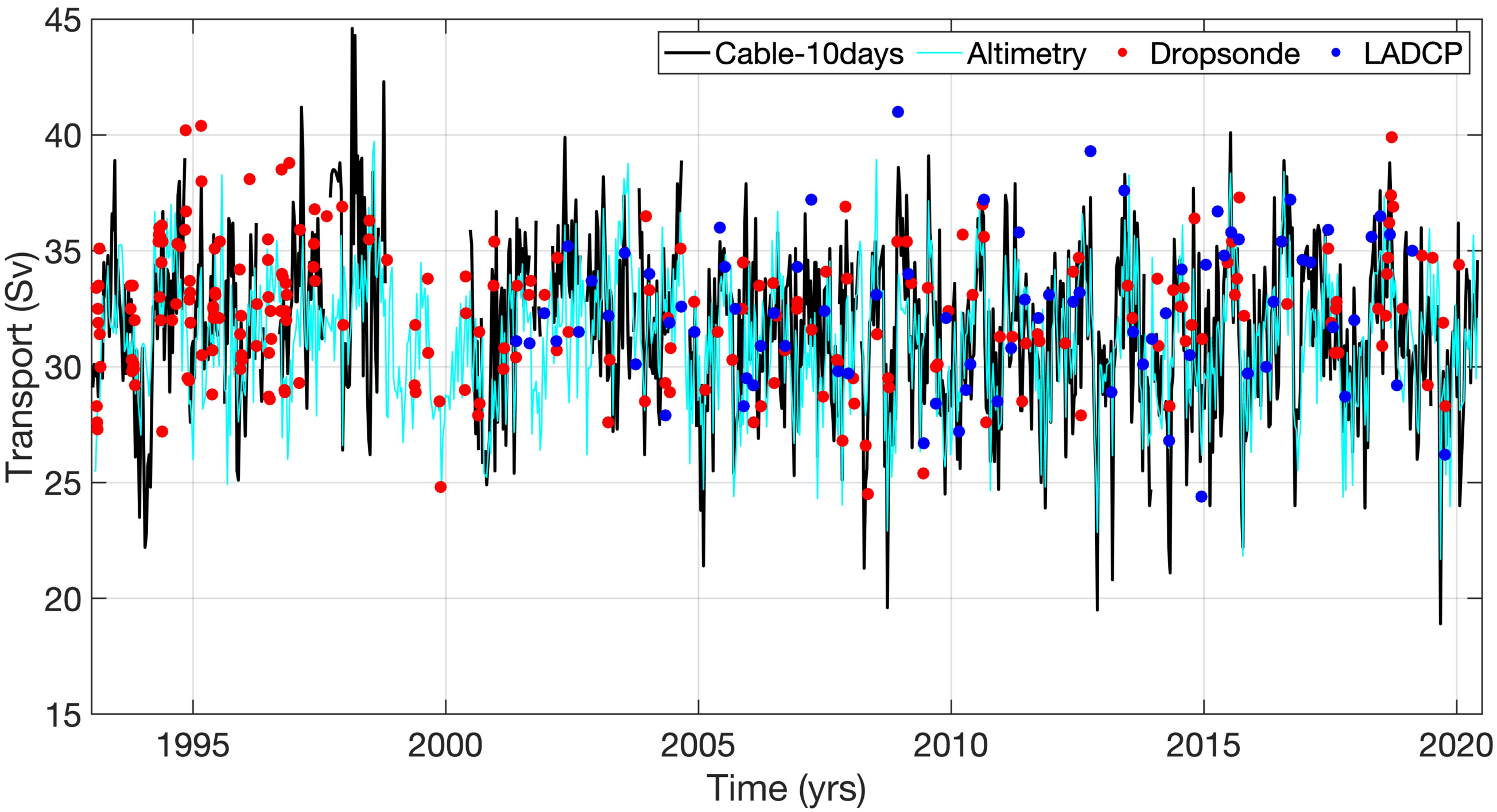


Figure 9.

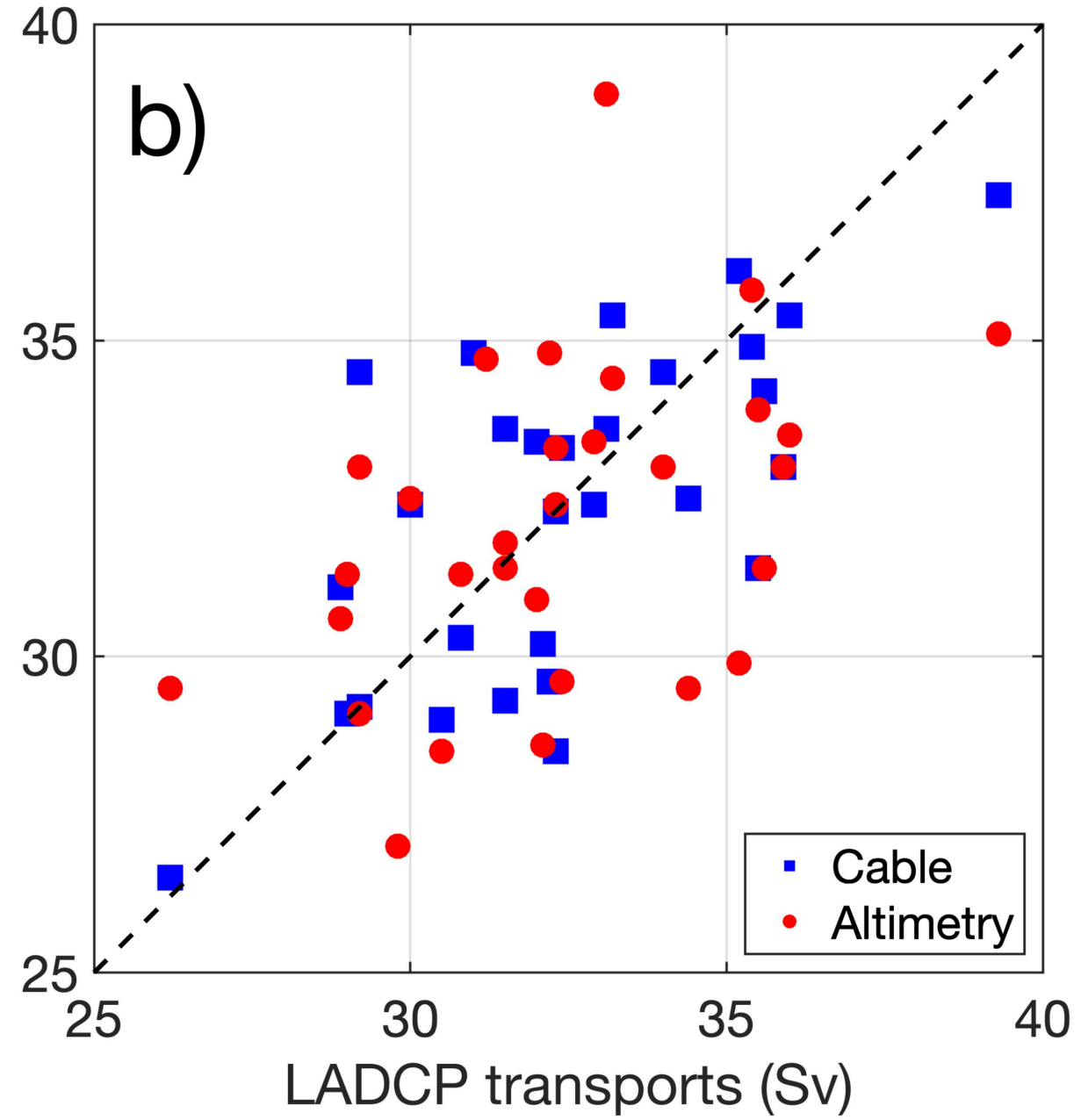
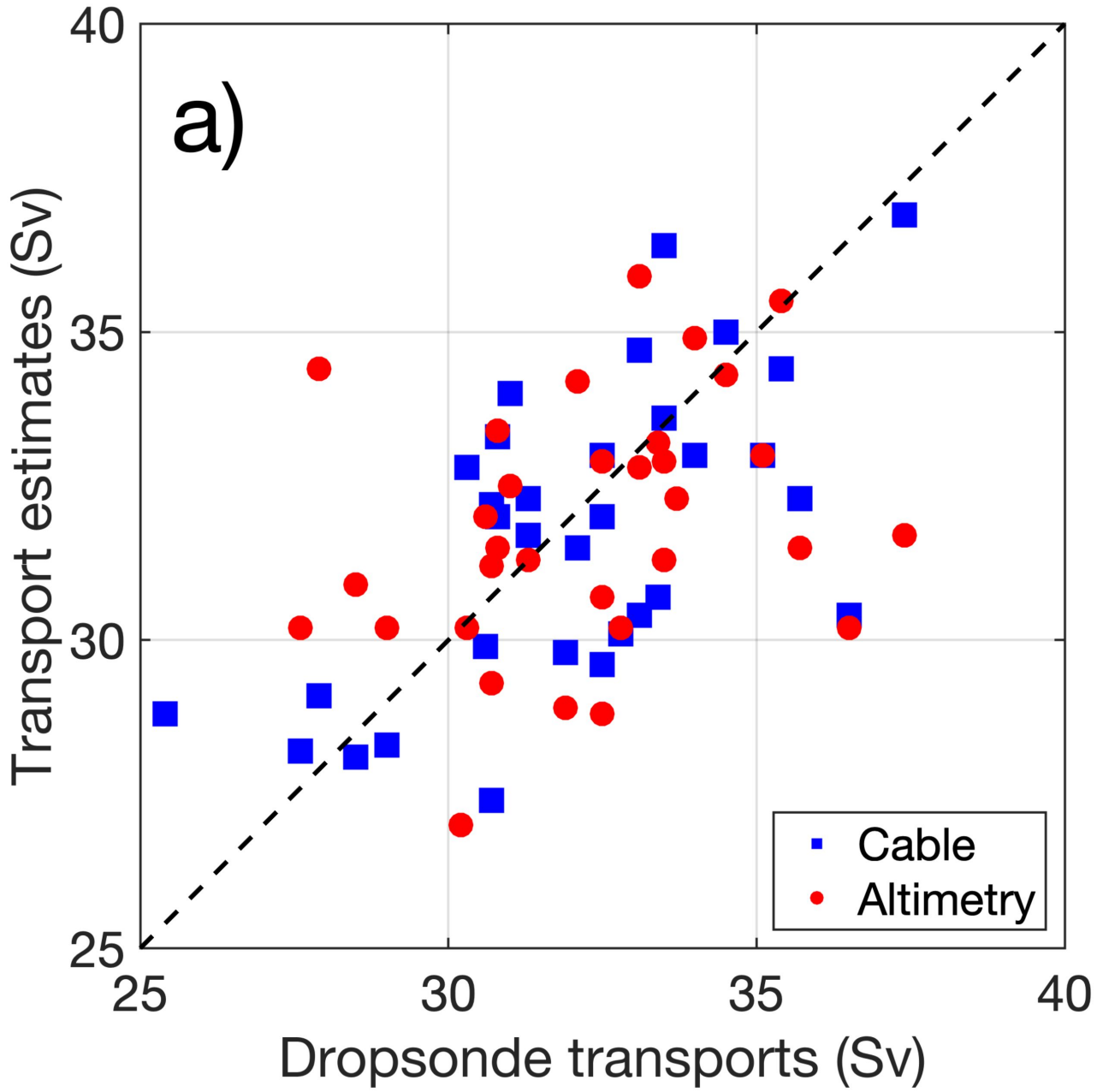


Figure 10.

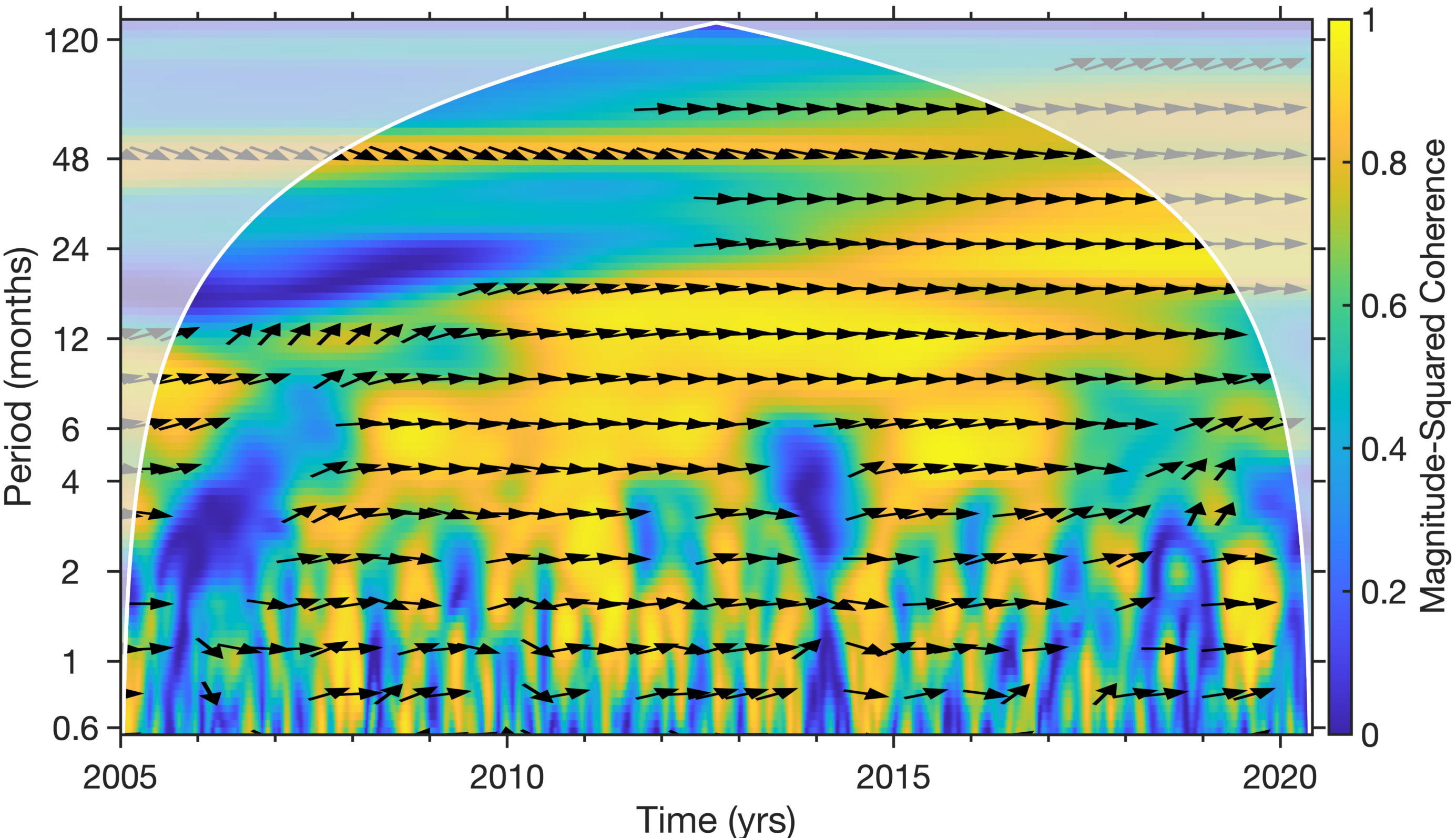


Figure 11.

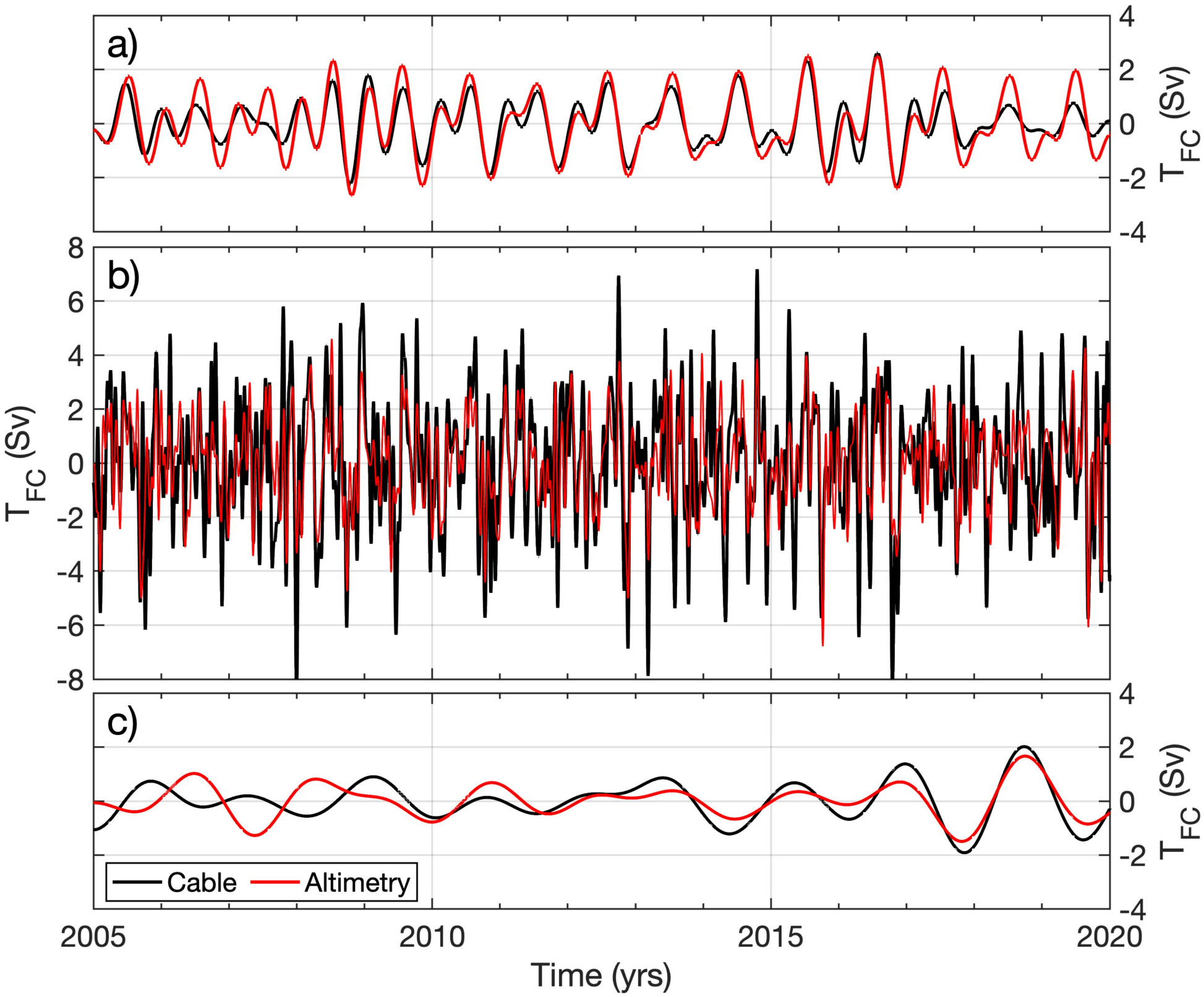


Figure 12.

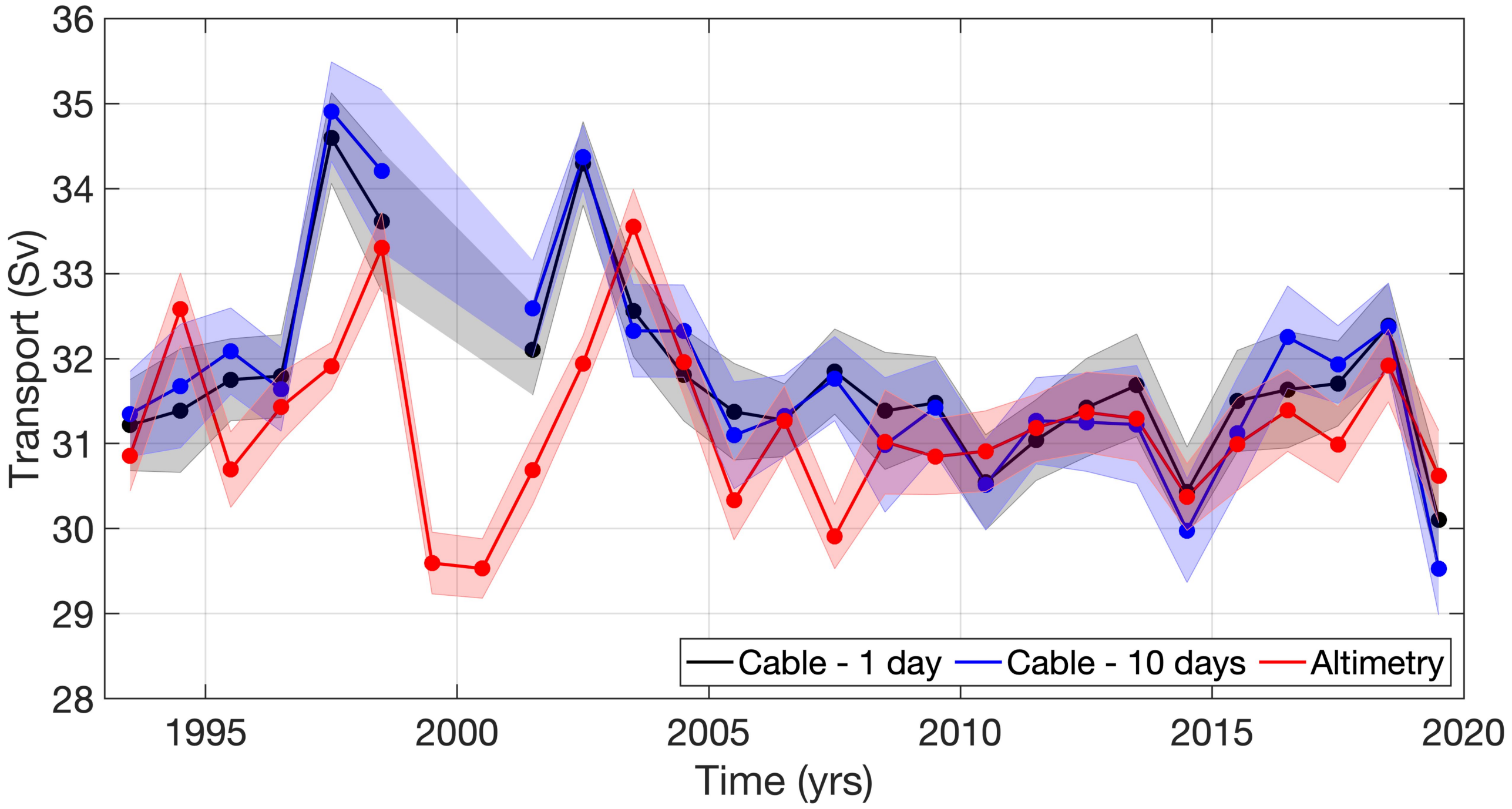


Figure 13.

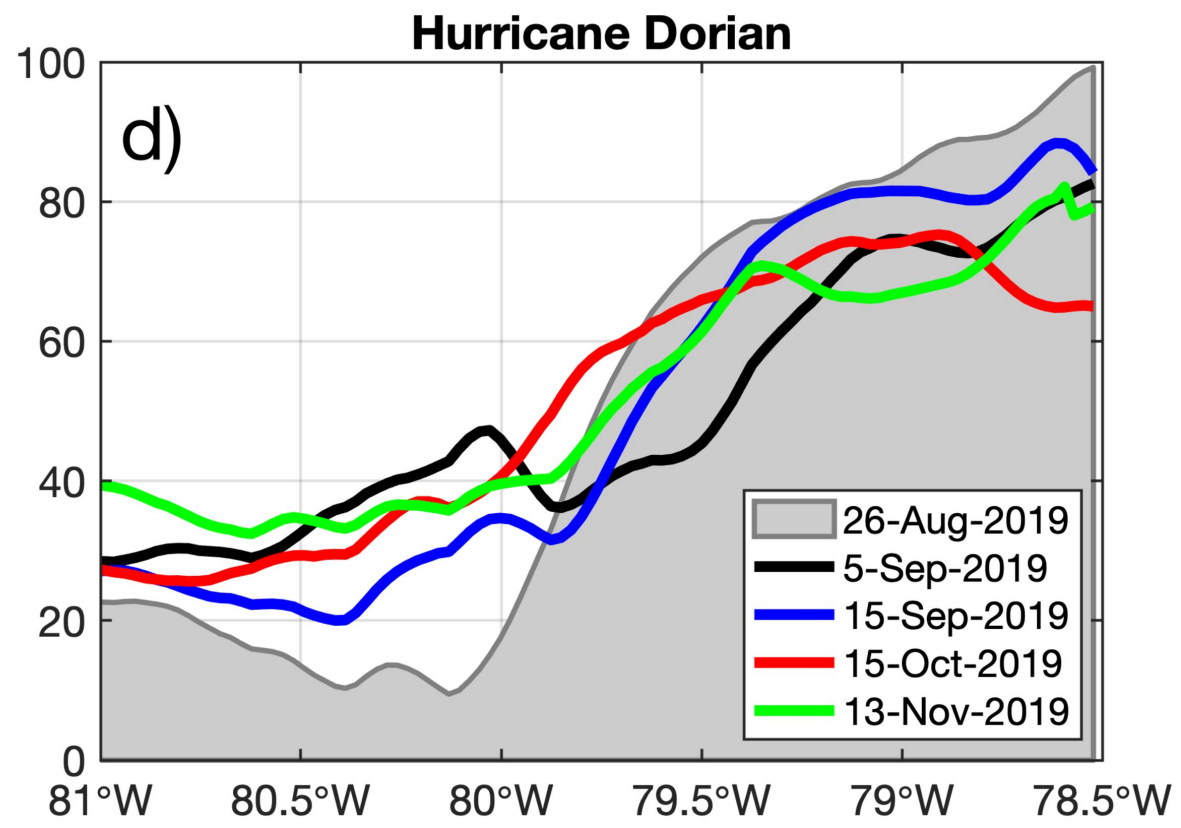
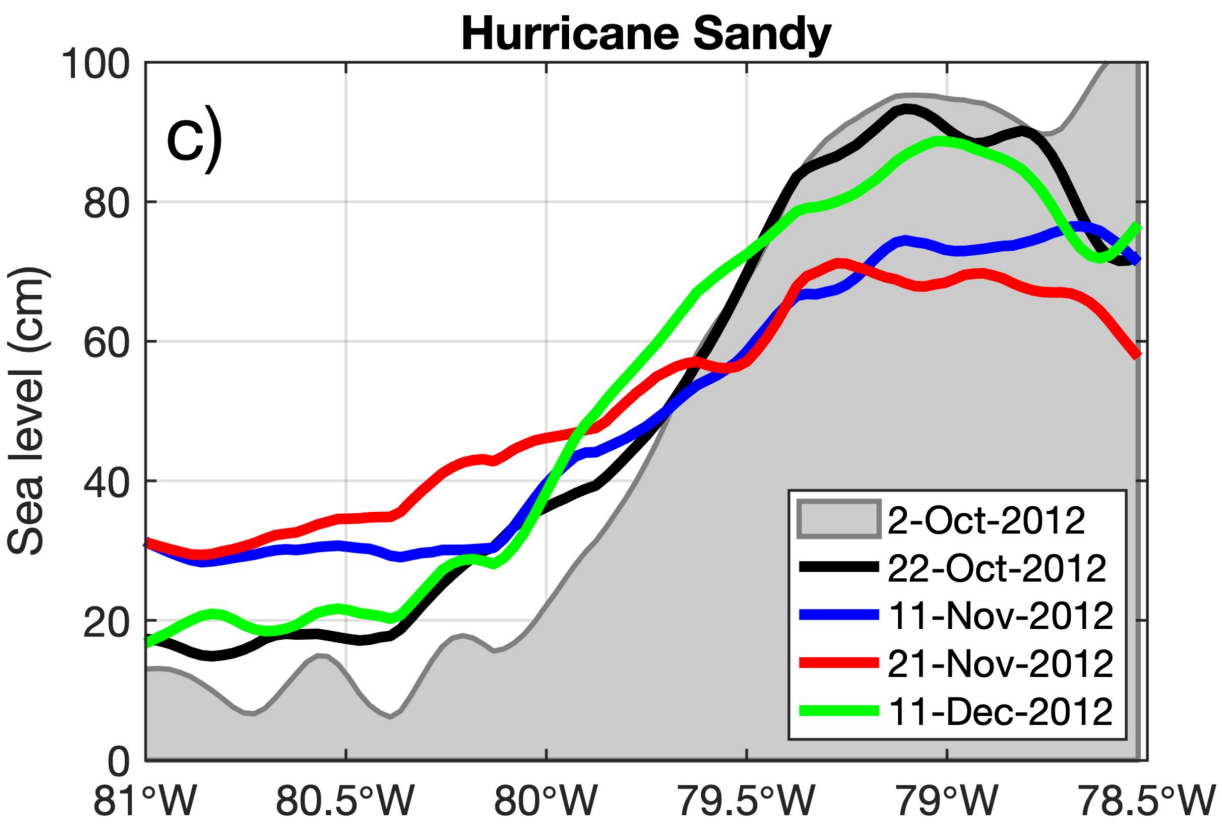
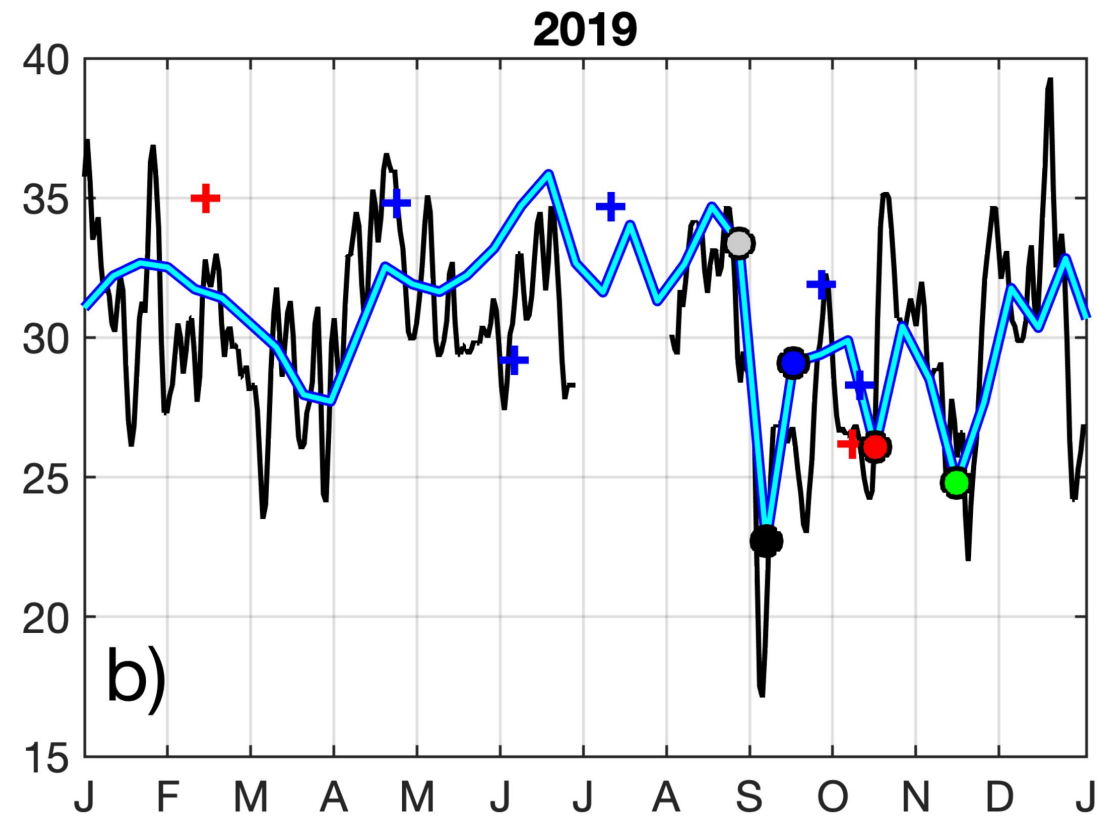
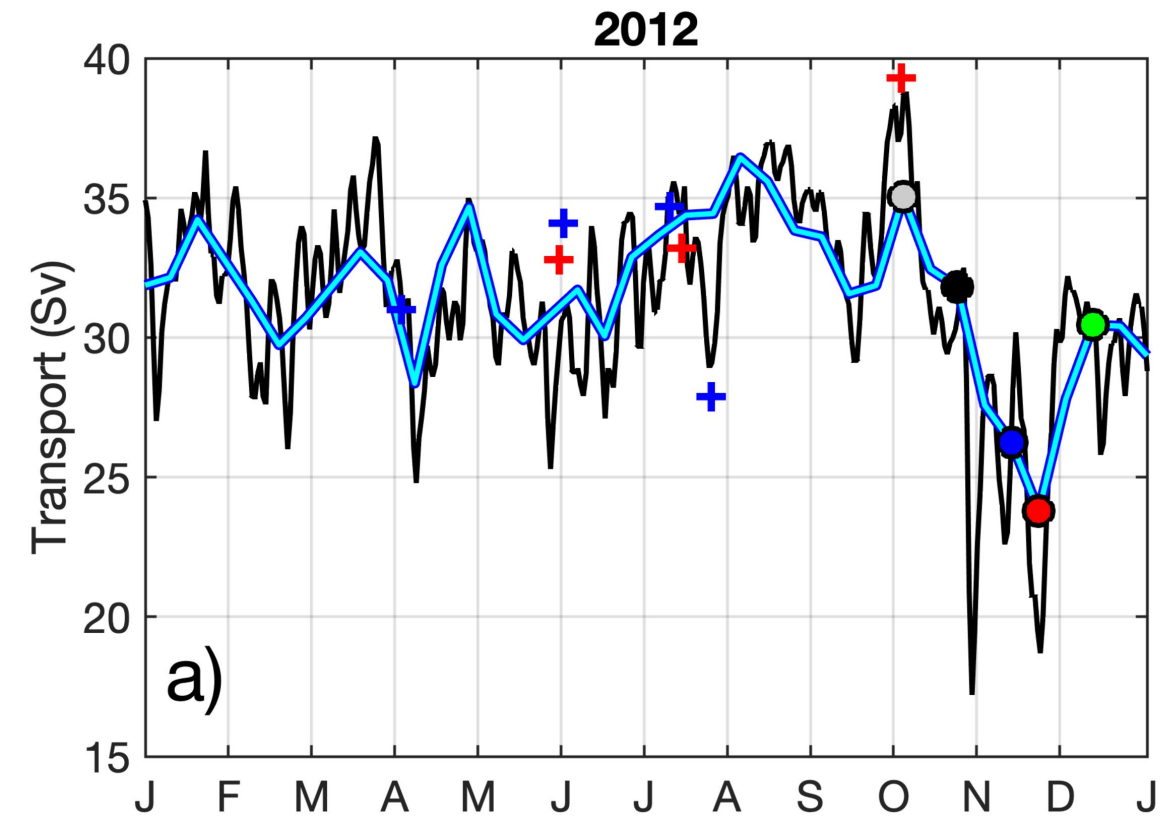


Figure 14.

